

Review

# The Tripodal Ligand's 4f Complexes: Use in Molecular Magnetism

Kira E. Vostrikova 

Nikolaev Institute of Inorganic Chemistry, Siberian Branch, Russian Academy of Sciences,  
630090 Novosibirsk, Russia; vosk@niic.nsc.ru

**Abstract:** A predictable type of coordination is a key property of tripodal ligands. Homo- and heteroleptic lanthanide complexes with tripodal ligands are a representative class of compounds. However, despite the fact that many of them are paramagnetic, their magnetic behavior is poorly studied. This is because their photophysical and catalytic properties are considered more attractive. In the present review, we try to summarize the available structural information and only a few examples of data on magnetic properties in order to draw some conclusions about the prospect of such ligands in the design of quantum molecular magnets involving lanthanide (Ln) ions. We would also like to catch the reader's attention to the fact that, despite the consideration of a large part of the currently known Ln compounds with tripodal ligands, this review is not exhaustive. However, our goal is to draw the attention of magnetochemists and theoreticians to a whole niche of air-stable Ln complexes that is still out of their field of vision.

**Keywords:** tripodal ligands; lanthanides; single-molecule magnets; single-ion magnets; axiality



**Citation:** Vostrikova, K.E. The Tripodal Ligand's 4f Complexes: Use in Molecular Magnetism. *Inorganics* **2023**, *11*, 307. <https://doi.org/10.3390/inorganics11070307>

Academic Editors: Leonor Maria and Joaquim Marçalo

Received: 12 June 2023

Revised: 7 July 2023

Accepted: 8 July 2023

Published: 20 July 2023



**Copyright:** © 2023 by the author. Licensee MDPI, Basel, Switzerland. This article is an open access article distributed under the terms and conditions of the Creative Commons Attribution (CC BY) license (<https://creativecommons.org/licenses/by/4.0/>).

## 1. Introduction

The rational design of coordination compounds with specific physical properties is a challenging task for synthetic chemists. Chemical engineering can be both highly specialized (improvement of a specific property) and focused on the preparation of polyfunctional materials. The most common objective for material scientists is to tune the electronic properties of a compound. This can be achieved by varying the ligand environment of the central atom, namely the polyhedron geometry and the ligand field strength. The latter is mainly defined by the donor atoms' composition, whereas the former depends not only on the geometry of the ligand, but also on the predictability of its coordination mode. The organic tripod molecules bearing donor atoms on each of their three legs are the best choice for the chemical design of different complexes with a given geometry. Moreover, the latter can be easily adjusted using the methods of synthetic organic chemistry. Therefore, it is not surprising that tripodal ligands are widely used in various fields of applied coordination chemistry, such as catalysis [1–6]; chemo sensing [7–9]; photo- [10–12] and electroluminescence [11,13,14]; molecular gears and motors construction [15,16]; biomedical applications [17–20]; and molecular magnetism [12,21–24].

Although numerous high-spin molecules based on tripodal ligands (including paramagnetic ones [25–32]) and d-metal ions have been studied to date [33–42], such studies for 4f elements have mainly been focused on synthesis, structural features, and the photophysical properties of the compounds with diamagnetic tripods, often leaving aside the study of their magnetic behavior [10,11,14,18,43–48]. The present review is devoted to an analysis of the known lanthanide complexes with tripodal ligands from the point of view of their application in the field of molecular magnetism.

## 2. Short Theoretical Background

Due to the slow attenuation of magnetization and the existence of magnetic hysteresis of purely molecular origin, single-molecule magnets (SMMs) could offer considerable future

applications in the domain of spintronics, quantum computing, and—especially—for use as materials for information storage at the molecular level. There are three main characteristics of SMMs: The first is the effective energy barrier ( $U_{eff}$ ), which provides magnetic bistability due to the spin reversal between the two ground states (GS). Highly efficient SMMs are very different in their behavior since large  $U_{eff}$  do not ensure that magnetization is kept at the elevated temperature during the period required for magnetic recording. This is defined by the second characteristic called blocking temperature ( $T_B$ ), which is a central claim for the implementation of SMMs in practice. Usually, spin–lattice relaxation and quantum tunneling of magnetization (QTM) lead to magnetization disappearance in an SMM. The first is associated with spin–phonon coupling, which can manifest itself through three different mechanisms: Orbach, Raman, and direct. The QTM is a temperature-independent phenomenon. A thermally assisted QTM process on excited states is also possible, and it is through this that relaxation occurs. These processes, phonon-type relaxation and QTM, which have been described in many papers [49–51], are closely related to the third SMM characteristic—relaxation time ( $\tau$ ). The  $U_{eff}$  value is ordinarily determined by the Arrhenius dependence of the relaxation time for the Orbach process. For the main SMM characteristic,  $T_B$ , the more common definition is that the magnetization blocking temperature is a temperature below which magnetic hysteresis opens. The stronger the SMM coercive field and the higher the residual magnetization in a zero magnetic field, the better magnetic bistability the magnetic material exhibits. In addition, higher  $U_{eff}$  and  $T_B$  provide quantized magnetization with satisfactory suppression of spin–lattice relaxation. To date, the achieved blocking temperatures are much lower than room temperature, which limits possible technological applications for the known SMMs [49–53]. Consequently, the quest for SMMs possessing large  $U_{eff}$  and  $T_B$  is a crucial issue in molecular magnetism. An important category of SMMs, lanthanide (Ln) single-ion magnets (SIMs—a subclass of SMMs including only mononuclear coordination compounds), are particularly promising due to their huge magnetic moments with immense magnetic anisotropy, which are caused by a large spin–orbit coupling being offered by the unquenched orbital momentum [54,55]. Improved  $T_B$  and  $U_{eff}$  are indispensable in terms of realizing their practical applications.

Almost thirty years of transdisciplinary investigations have resulted in SIMs with a record  $U_{eff}$  (up to 2000 K) and a  $T_B$  near liquid nitrogen temperature [56–59]. This is a result of several approaches, which have shown that enhancing the uniaxiality of magnetic anisotropy is crucial for the design of highly performing SIMs [60–64]. The uniaxiality of SIMs can be provided by the corresponding symmetry of the coordination polyhedron. However, despite the similarity in chemical behavior (due to the shielded nature of the f-electrons), Ln<sup>3+</sup> cations are very different in terms of their electronic properties. This leads to the fact that for ions differing in electronic configurations, their ligand environment must be taken into account along with the crystal field (CF) splitting. Among the lanthanides, the trivalent Tb, Dy, Ho, and Er can produce ground states (GS) with large  $m_J$ —if the appropriate CF is provided [65]. This is because the electronic clouds of Ln GS have different shapes. The letters are generally subdivided into prolate and oblate spheroid types [60,66–68], which require, respectively, different ligand field organization: axial for Pr, Tb, Dy, and Nd, and equatorial for Pm, Tm, Yb, and Er [60,69]. Thus, to increase the energy barrier  $U_{eff}$ , the symmetry of an Ln<sup>3+</sup> ion environment along with the ligand field approach (axial or equatorial) are required, depending on the nature of the Ln<sup>3+</sup> [70,71]. Although this provides an opportunity to design SMMs with ground states that have a large magnetic moment, relaxation often occurs through excited states that have different electron densities. In addition, the energy gap separating the  $m_J$  levels (a key parameter for SMM enhancement) is difficult to forecast until a quantitative approach is applied and the mechanisms of relaxation are entirely established.

If strong intermolecular exchange interactions are absent between the mononuclear SIMs (which is precisely the case for lanthanide ions since the magnetic electrons are on a well-screened 4f shell), then the ligand field surrounding the magnetic metal ions leads to the degeneration of the  $^{2S+1}L_J$  multiplets, resulting in  $2J + 1$  sublevel  $m_J$ . This

results in a highly anisotropic ground spin state, which can be explained using quantum mechanics. However, we will not immerse the reader in the mathematical details for all types of magnetic anisotropy, as they can be found in the literature [72–74]. Given a fixed molecular structure, uniaxial anisotropy is important to suppress QTM and decrease thermo-assisted magnetic relaxation. In addition, a source of under-barrier QTM is the transversal anisotropy caused by transverse CF, which should be avoided in the design of SIMs. Tong et al. [75] have studied the influence of symmetry on the transverse terms. They conclude that the  $C_{\infty v}$ ,  $C_{5h}/D_{5h}$ ,  $S_8/D_{4d}$ , and  $S_{12}/D_{6d}$  point group symmetries vanish terms  $B_k^q$  ( $q \neq 0$ ) of CF for interested  $Ho^{3+}$  ions, resulting in the perfect uniaxial anisotropy. Thus, by adjusting the coordination polyhedron symmetry and the ligand environment for a particular lanthanide center, QTM in a single-ion magnet can be overcome.

However, even the most accurate theoretical predictions are not easy to implement in practice since, in order to obtain a coordination polyhedron with a certain symmetry, it is necessary to use ligands with a predictable manner of coordination. Therefore, when designing any SIM, synthetic chemists have to compromise between polyhedra with uniaxial symmetry and a specific choice of ligands to construct magnetic molecules.

Therefore, the analysis of currently known molecular mononuclear complexes containing tripodal ter- and tetradentate ligands is aimed at drawing the attention of the scientific community to the use of such ligands in the design of Ln complexes with uniaxial anisotropy. To date, approaches based on the shape of 4f electron clouds (oblate or prolate) have been developed to select the most suitable Ln-ions for an appropriate ligand field for both the ground state and the excited levels of the central atom [60,76–78].

### 3. Lanthanide Complexes with Tripodal Ligands

#### 3.1. Complexes with Pyrazolyl-Bearing Tripodal Ligand

##### 3.1.1. Complexes with Tris(Pyrazolyl)Borates Tripodal Ligands

The first and most studied coordinative tripods were the scorpionate ligands, hydrotris(pyrazolyl)borates, first obtained by S. Trofimenko [33,35]. The coordination chemistry of these negatively charged ligands mainly includes d-metal complexes [37,79,80]. In the chemistry of coordination-capacious f-elements, scorpionates are often used as capping ligands that additionally compensate for the positive charge of Ln [81–86]. In the area of molecular magnetism, the bulky hydro-tris(pyrazolyl)-borates (TPzB) are commonly employed as a capping ligand to reduce intermolecular magnetic interactions and protect the air-sensitive radical sites [87]. A number of 3d ion-based SMMs and SCMs (single-chain magnets) [88,89] have been obtained using this approach. Unfortunately, very few Ln-TPzB complexes have been magnetically studied. Among them, there are three  $Dy^{3+}$  compounds: a purely homoleptic  $[Dy(Tp^{Me_2})_2]I$  (**1**), a heteroleptic  $(Me_4N)[DyCl_3(Tp^{Me_2})]$  (**2**) ( $Tp^{Me_2}$  = tris(3,5-dimethylpyrazolyl)borate), and a mixed-type complex  $[Dy(Tp^{Me_2})_2][DyCl_3(Tp^{Me_2})] \cdot CH_2Cl_2$  (**3**) [90]. The  $Dy^{3+}$  ions are six-coordinated for all three complexes (Figure 1). The  $[Dy(Tp^{Me_2})_2]^+$  cation in **3** adopts a bent sandwich-type structure with a B–Dy–B angle of  $169.57(3)^\circ$  [90]. In the cationic part, the  $Dy^{3+}$  center is surrounded only by N-atoms of two  $Tp^{Me_2}$ , while in the anionic part, the coordination sphere of  $Dy^{3+}$  consists of the three nitrogen atoms from one tripod and the three chloride ions. The structural shape analysis has shown that the Dy center in cation **3** is in an elongated trigonal antiprismatic coordination environment (Figure 1) [90]. Such a geometry has been previously found for the divalent lanthanides [44,46,91].

The complex **2** contains the separate  $[DyCl_3(Tp^{Me_2})]^-$  anion, which is alike to that of the complex **3** but it has  $Me_4N^+$  as a cation. Compound **1** is isomorphous to the  $Sm^{3+}$  analogue reported earlier [44]. It contains well-isolated  $[Dy(Tp^{Me_2})_2]^+$  and iodide ions. The cation in **1** is placed in a 2/m symmetry element representing a mirror plane passing through two of the pyrazolyl rings [90]. It is worthy of note that the Dy center in **1** has a similar geometry comparatively to those of compound **3**, but it has the following key dissimilarities: the two independent Dy–N bond distances, 2.376(2) and 2.430(3) Å, are longer compared to those of **3**; due to the crystallographic symmetry, the two planes defined

by the nitrogen donor atoms of each tripod are parallel, whereas in **3**, the angle between the planes is  $10.53(2)^\circ$ ; both the  $\text{Tp}^{\text{Me}_2}\text{-Dy-Tp}^{\text{Me}_2}$  and  $\text{B-Dy-B}$  angles in **1** ( $178.64(2)^\circ$  and  $180.00(2)^\circ$ ), are broader than those of **3** ( $173.05(2)^\circ$  and  $169.57(2)^\circ$ ), indicating that cation **1** reveals a more dense and linear structure than the cation in **3**. In conclusion, the isolated  $[\text{DyCl}_3(\text{Tp}^{\text{Me}_2})]^-$  is in an alike trigonal antiprismatic coordination environment with very similar bond distances and angles for the compounds **2** and **3** [90].

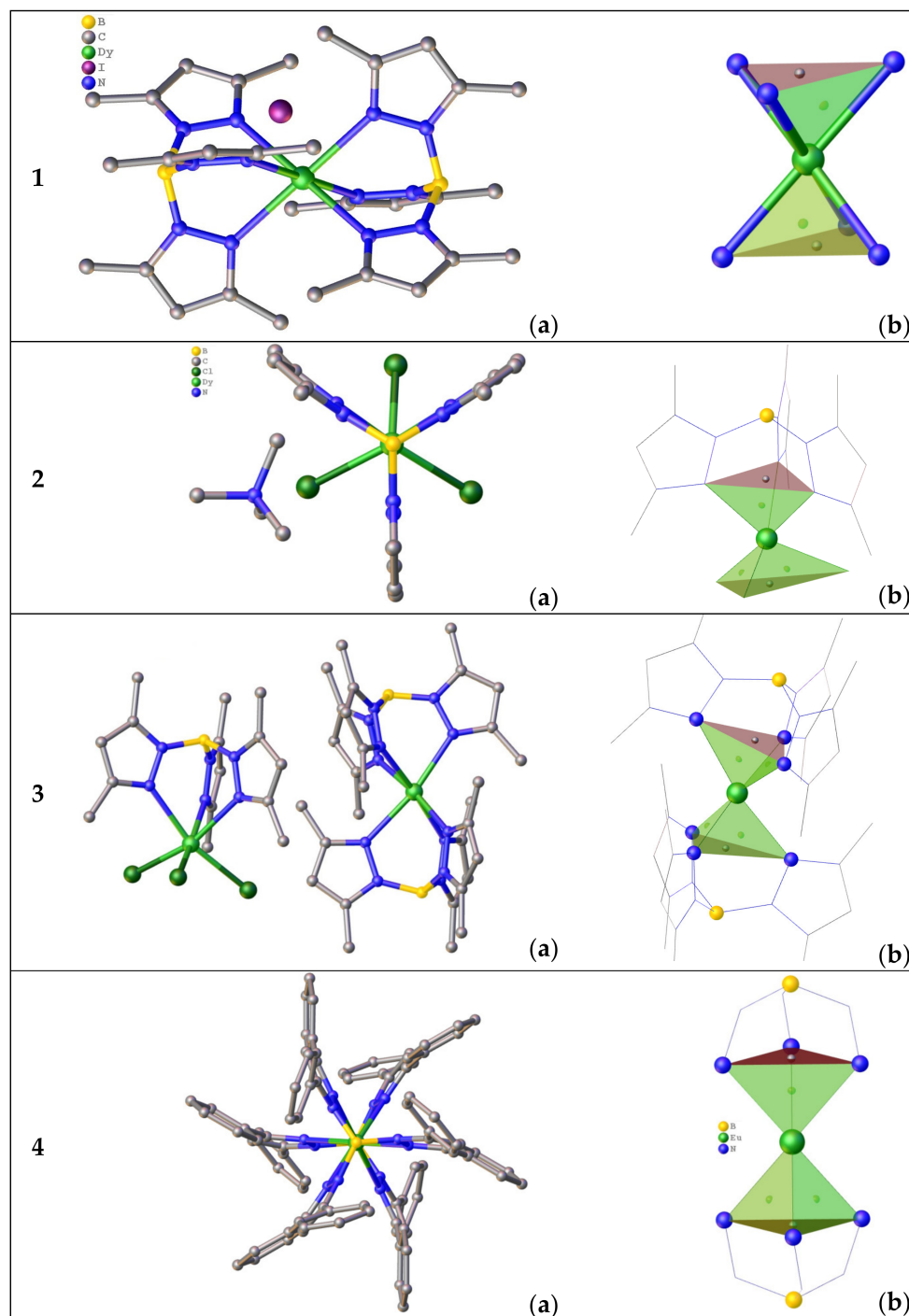


**Figure 1.** Molecular structures (a) and trigonal antiprismatic coordination polyhedra (b) for the compounds **1–4**. Hydrogen atoms are omitted. The picture was made using open crystallographic data.

Magnetic studies have shown that complex **1** displays an energy barrier  $U_{eff}$  of 13.5 K with  $\tau_0 = 1.6 \times 10^{-6}$  s under a 0.08 T applied field, while **3** is an SIM with  $U_{eff} = 80.7$  K and  $\tau_0 = 6.2 \times 10^{-7}$  s under a zero applied field [90]. The results of the first principle CASSCF + RASSI-SO calculations correspond well with the experimental magnetic measurements for **3** and **1**, indicating the presence of an intermolecular dipolar interaction of  $\langle zJ \rangle = -0.1 \text{ cm}^{-1}$  in **3** [90]. The absence of SMM behavior in **1** and **2** under a zero dc field supports the conclusion that the slow magnetic relaxation observed for **1** is a result of minor changes in the coordination geometry of the  $\text{Dy}^{3+}$  ion, and/or intermolecular dipolar interactions between the anionic and cationic moieties [90]. The QTM probability of a ground state for Kramers doublets is described by the crystal field (CF,  $B_k^q$ ) parameters. QTM is prevailing when the non-axial terms (for which  $q \neq 0$  and  $k = 2, 4,$  and  $6$ ) are larger compared to the axial ones (for which  $q = 0$  and  $k = 2, 4,$  and  $6$ ). For all the  $\text{Dy}^{3+}$  ions in **1–3**, there is significant transverse anisotropy and fast QTM relaxation [90]. The cationic Dy1 units in **1** and **3**, however, have a relatively small temperature assisted-QTM in the first excited states. This can assist magnetization relaxation via the first excited states when a dc field is applied [90].

From the point of view of the design of high-performance SIMs, it is worth paying special attention to the recent publication by Hao Qi et al. [92], which is devoted to the synthesis of the Eu(II) compounds with bulky tris-pyrazolyl-borates. First of all, it should be noted that the obtained three complexes are stable under ordinary conditions and can be sublimated. Both of these properties are very important for practical applications. When extending the synthesis procedure chosen by the authors to magneto-anisotropic Ln ions, it would be interesting to test these compounds for SMM behavior. The complexes  $\text{Eu}(\text{Tp}^{\text{Ph,Me}})_2$ ,  $\text{Eu}(\text{Tp}^{\text{Ph}})_2$ , and  $\text{Eu}(\text{Tp}^{\text{Ph}_2})_2$  are all hexa-coordinated, with six N atoms from pyrazole hetero-cycles.  $\text{Eu}(\text{Tp}^{\text{Ph}})_2$  is isomorphous to the known compounds  $\text{Sm}(\text{Tp}^{\text{Ph}})_2$  and  $\text{Yb}(\text{Tp}^{\text{Ph}})_2$  [44]. The molecular structure of  $\text{Eu}(\text{Tp}^{\text{Ph}_2})_2$  differs from that of  $\text{Eu}(\text{Tp}^{\text{Ph,Me}})_2$  and  $\text{Eu}(\text{Tp}^{\text{Ph}})_2$ . Due to the substituent changes, the structure symmetry of the compounds rises in the following order  $\text{Eu}(\text{Tp}^{\text{Ph,Me}})_2 \rightarrow \text{Eu}(\text{Tp}^{\text{Ph}})_2 \rightarrow \text{Eu}(\text{Tp}^{\text{Ph}_2})_2$ . The latter has a higher symmetry of  $D_{3d}$ , while the others possess a “bent sandwich-like” structure known for other Ln(II) ions [91,93–98]. The complex  $\text{Eu}(\text{Tp}^{\text{Ph}_2})_2$  (**4**) adopts an ideal trigonal antiprismatic ( $D_{3d}$  symmetry) molecular structure with a linear B–Eu–B fragment (Figure 1).

The  $D_{3d}$  single-point group with a  $C_3$  axis is a subgroup of  $D_{6h}$ , which is effective enough to induce strong magnetic axiality in the Ln complexes [99–102]. However, trigonal antiprismatic complexes are underexplored in the field of molecular magnetism. This is especially true for the stable  $\text{Ln}^{2+}$  complexes of type **4**. However, one must take into account the ground state electronic configuration of the central ion when choosing a lanthanide for such studies. This is because the  $\text{Ln}^{2+}$  ions can have two types electronic configurations:  $4f^{n+1}5d^06s^0$  (for Nd, Sm, Eu, Dy, Tm, and Yb) and  $4f^n5d^16s^0$  (for La, Ce, Pr, and Gd) [103]. The letters should be avoided in the design of new, performant SIMs due to the presence of an unpaired electron at the 5d level.

### 3.1.2. Complexes of Tris(3,5-dimethylpyrazolyl)methane

The next group of tripods is a family of trispyrazolylmethane derivatives. In contrast to their boron-containing congener, tris(3,5-dimethylpyrazolyl)borate anion, trispyrazolylmethane terdentate ligands are neutral in most currently known compounds  $[\text{Ln}(\text{TPM})(\text{anion})_3]$  (TPM = tris(3,5-dimethylpyrazolyl)methane). For the first time, air-stable lanthanide complexes with TPM were obtained in 2007 by Sella et al. [45]. The six-coordinated compounds  $[\text{Ln}(\text{TPM})\text{Cl}_3](\text{CH}_3\text{CN})_2$  were prepared in an acetonitrile solution for  $\text{Ln}^{3+} = \text{Y}, \text{Ce}, \text{Nd}, \text{Sm}, \text{Gd},$  and  $\text{Yb}$ . The crystal structure was reported only for the  $\text{Y}^{3+}$  ion. The molecular structure of  $[\text{Y}(\text{TPM})\text{Cl}_3](\text{CH}_3\text{CN})_2$  (**5**) is shown in Figure 2.

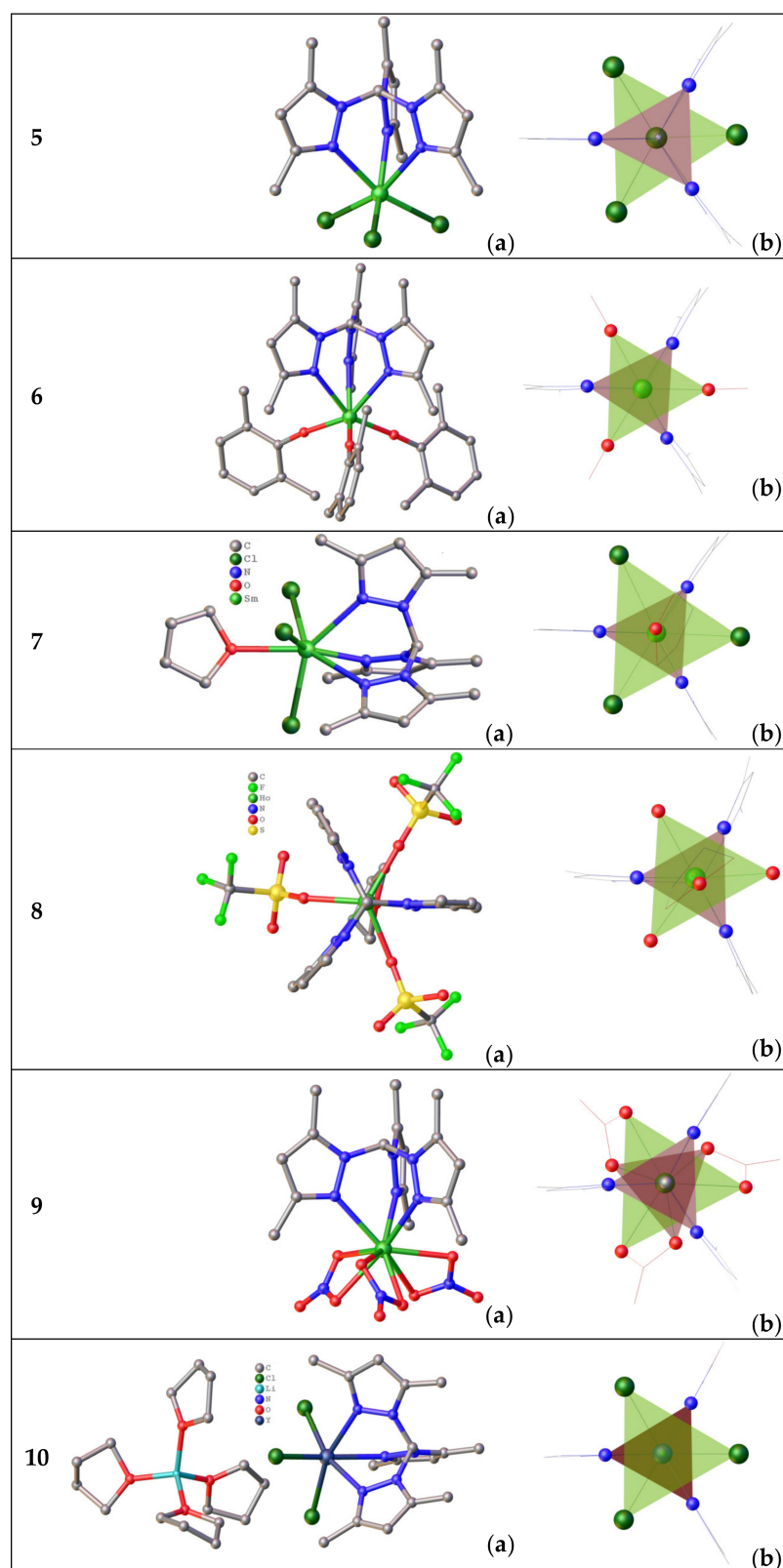


**Figure 2.** Molecular structures (a) and trigonal antiprismatic coordination polyhedra (b) for the compounds 5–10. Hydrogen atoms are omitted. The picture was made using open crystallographic data.

Long et al. [24] have since studied the isostructural of the yttrium congener complexes for  $\text{Tb}^{3+}$ ,  $\text{Dy}^{3+}$ , and  $\text{Er}^{3+}$  with the same composition. The compounds crystallize in the

space group  $P2_1/n$  with two solvent molecules. A SHAPE [104] analysis revealed that the coordination environment of  $\text{Ln}^{3+}$ -ions is a distorted octahedron.

The isomorphous  $[\text{Ln}(\text{TPM})(\text{OArMe}_2)_3](\text{thf})_3$  ( $\text{Ln} = \text{Y}, \text{Nd}, \text{Sm}$ , and  $\text{ArMe}_2 = \text{Ph-2,6-Me}_2$ ) were obtained in a concentrated THF solution at  $-30^\circ\text{C}$ . These complexes crystallize in the space group  $P-1$  with three solvent molecules. The molecular structure of the  $[\text{Sm}(\text{TPM})(\text{OArMe}_2)_3](\text{thf})_3$  (**6**) is shown in Figure 2. In all three compounds, each six-coordinated Ln-ion is in a trigonal antiprismatic coordination environment ( $C_3$  symmetry) composed of one smaller triangle (formed by nitrogen atoms) and a larger one that has the  $\text{OAr}^{\text{Me}_2}$  groups in its vertices. This is clearly seen by comparing the  $\angle(\text{N-Ln-N})$  and  $\angle(\text{X-Ln-X})$  angles ( $\sim 70$  vs.  $100\text{--}108^\circ$ ). It should be noted that in the  $[\text{Ln}(\text{TPM})(\text{OAr}^{\text{Me}_2})_3]$  compounds, the Ln–N distances (2.565(5) Å) are longer than those in **5** (2.459(5) Å), suggesting that the binding of the TPM tripod is subtle to modifications in the steric demand of the adjacent ligands in the Ln coordination sphere. Compared with the six-coordinate compounds comprising the isosteric but anionic  $\text{Tp}^{\text{Me}_2}$  tripods, the average M–N distance is also noticeably longer (2.44(1) and 2.443(7) Å) in  $[\text{Sm}(\text{Tp}^{\text{Me}_2})_2]\text{BPh}_4$  and  $[\text{Sm}(\text{Tp}^{\text{Me}_2})_2]\text{I}$  [44], which is consistent with the weaker Ln interaction with a neutral ligand.

The molecular structure of seven-coordinate  $[\text{Sm}(\text{TPM})\text{Cl}_3(\text{thf})]\cdot\text{thf}$  (**7**) is presented in Figure 2. By contrast to the unsolvated six-coordinate complex **5**, **7** contains one thf ligand, which can probably be accommodated due to the larger coordination sphere of the Sm-ion than that of Y. The two studied  $[\text{Ln}(\text{TPM})(\text{OTf})_3(\text{thf})]$  complexes are isomorphous due to almost the same ionic radii of  $\text{Y}^{3+}$  and  $\text{Ho}^{3+}$ . The molecular structure for the latter, (**8**), is demonstrated in Figure 2. The coordination sphere of the triflate or chloride complexes  $[\text{Ln}(\text{TPM})(\text{X})_3(\text{thf})]$  may be described differently. Firstly, a trigonal antiprism is defined by one tripod and three anionic ligands ( $\text{X} = \text{Cl}$  or  $\text{OTf}$ ), with a thf-ligand lying on the  $C_3$  axis passing through the top of the tripod and the triangular face defined by the anions. Secondly, a tricapped trigonal pyramid has three N atoms of the TPM lying in the triangular base, with the thf oxygen defining the apex [45]. As in the case of the six-coordinate compounds, the triangles defined by nitrogen are smaller than those defined by the three anionic ligands.

Much later, the three isomorphous complexes  $[\text{Ln}(\text{TPM})(\text{NO}_3)_3]\cdot\text{MeCN}$  ( $\text{Ln}^{3+} = \text{Tb}, \text{Dy}$ , and  $\text{Er}$ ) were synthesized and studied, which crystallize in the  $P2_1/n$  space group with one heteroleptic  $[\text{Ln}(\text{TPM})(\text{NO}_3)_3]$  complex in the asymmetric unit [24]. The molecular structure of the complex  $[\text{Ln}(\text{TPM})(\text{NO}_3)_3]\cdot\text{MeCN}$  (**9**) is presented in Figure 2. The coordination sphere of **9** is composed of three nitrogens from the tripodal ligand and six oxygens from bidentate nitrate anions. The Tb–N distances ranging from 2.482(2) to 2.530(2) Å are slightly longer than the Tb–O ones (2.416(2)–2.458(2) Å). The analysis of the nine-coordinate polyhedron by the SHAPE software indicates that the geometry of the lanthanide site could be best described as a spherical tricapped trigonal prism [24].

Magnetic studies for the TPM coordination compounds were performed only for the two types of anionic co-ligands (chloride and triflate) for the three  $\text{Ln}^{3+}$  ions: Tb, Dy, and Er, which are congeners of the compounds **5** and **8**. For these complexes, the room temperature  $\chi T$  values correspond well to the theoretical ones predicted for a single  $\text{Ln}^{3+}$  ion consuming the free ion approximation. A temperature decrease induces a negative deviation of  $\chi T$  for all the compounds, reflecting the depopulation of the  $m_j$  states [24]. The magnetization for both series does not saturate even at a field of 7 T, witnessing the pronounced magnetic anisotropy for all six complexes. Field-induced slow magnetic relaxation was observed for all nitrate compounds and only for the Er congener of **5**. Based on these studies, the authors argue that the manifestation of a field-induced slow magnetization relaxation is greatly reliant on the anion's nature. While nitrate moieties appear to be suitable to stabilize the oblate electronic density of  $\text{Dy}^{3+}$ , chloride ions generate an equatorial crystal field, allowing the slow relaxation of prolate  $\text{Er}^{3+}$  ions [24].

### 3.1.3. Complexes of Anionic Tripodal Ligand: Tris(3,5-dimethylpyrazolyl)-methanide

The electronic analog of tris(3,5-dimethylpyrazolyl)borate anion is a deprotonated TPM: tris(3,5-dimethylpyrazolyl)-methanide (TPM<sup>\*</sup>). Only a few Ln complexes of TPM<sup>\*</sup> are known to date [105]. Among them, the three complexes with diamagnetic central Ln<sup>3+</sup> ions [Ln(TPM<sup>\*</sup>)Cl<sub>3</sub>][Li(thf)<sub>4</sub>] (Ln = Sc, Y (**10**), Lu) were synthesized and structurally characterized. The molecular structure of [Y(TPM<sup>\*</sup>)Cl<sub>3</sub>][Li(thf)<sub>4</sub>] (**10**) is shown in Figure 2. All complex anions have C<sub>3</sub> symmetry, and each metal ion is surrounded by three N atoms of the TPM<sup>\*</sup> ligand and three chloride anions, which form a distorted octahedron polyhedron that is also found for **5**, despite the different space groups: *P*2<sub>1</sub>/*n* and *R*<sub>3</sub> for **5** and **10**, respectively. It should be emphasized that the Y–N bond lengths of 2.425(5) Å for [Y(TPM<sup>\*</sup>)Cl<sub>3</sub>]<sup>−</sup> (in **10**) are somewhat shorter compared to those in the anions [Y(TPM)Cl<sub>3</sub>]<sup>−</sup> and [Tb(TPM)Cl<sub>3</sub>]<sup>−</sup> 2.459(2) Å [45], and 2.472(3)–2.490(3) Å [24]), but are closer to those of 2.425(6) Å for DyCl<sub>3</sub>(Tp<sup>Me</sup><sub>2</sub>)<sup>−</sup> [90]. This makes sense since the tripodal ligand in both the latter and in **10** has a negative charge, while the tripod in the complexes with longer Ln–N bonds is neutral.

To our great regret, we could not find a single publication describing the magnetic properties of methanide-containing complexes of paramagnetic lanthanides.

### 3.2. Complexes with the Pyridyl-Bearing Tripodal Ligands

Pyridine-containing tripodal ligands have been described earlier [1]. Moreover, a diversity of bridgehead atoms such as nitrogen, carbon, and phosphorus [106], as well as other elements: Si [107], As [108], Al and In [109], Sn [110,111], Pb [112], and B [113] have been included to alter the properties of the coordination metal complexes, both in terms of polyhedral geometry and to tune the electronic structure.

Strangely enough, the structurally characterized lanthanide complexes of the tris(2-pyridyl)methane have not yet been obtained. Only a small group of exotic organometallic complexes based on tris(2-pyridyl)metalates that are unstable under normal conditions have been obtained and structurally characterized. This family of Ln complexes will be briefly discussed in the next subparagraph of the review.

#### 3.2.1. Complexes of Tris(2-Pyridyl)Metalates

The most numerous group of the Ln complexes including tris(2-pyridyl)metalates are the coordination compounds of anionic tris(pyridyl)stannate (TPS) [114–117].

Interactions of [Ln(η<sup>5</sup>-C<sub>5</sub>Me<sub>5</sub>)<sub>2</sub>(OEt<sub>2</sub>)] with the lithium complex [LiSn(2-Py-5-Me)<sub>3</sub>(thf)] in THF solution using a 1:2 ratio gives sandwich-like [Ln{Sn(2-Py-5-Me)<sub>3</sub>}<sub>2</sub>] (**11**) complexes for divalent Ln = Eu and Yb [114]. The formation of **11** displays a more pronounced steric demand of the tripodal stannate ligand than C<sub>5</sub>Me<sub>5</sub> groups. This is comparable with similar reactions of tris(pyrazolyl)hydroborates [HB(R<sub>2</sub>pz)<sub>3</sub>]<sup>−</sup> (R = H, Me; pz = pyrazolyl) with [Ln(η<sup>5</sup>-C<sub>5</sub>Me<sub>5</sub>)<sub>2</sub>] species giving the analogous Ln<sup>II</sup> complexes [Ln(HB(R<sub>2</sub>pz)<sub>3</sub>)<sub>2</sub>] [114].

Both compounds of **11** crystallize in the same space group *P*2<sub>1</sub>2<sub>1</sub>2<sub>1</sub> and have very close cell parameters. The molecular structure for the europium complex is shown in Figure 3.

The Ln atoms of **11** are in a distorted octahedral coordination environment formed by six pyridyl nitrogens with a staggered organization of the pyridine rings around the Ln center. The coordination sphere around the Ln center is strongly distorted, and the large size of the Ln atom affords a slight twisting of one of the pyridine rings of each Sn(2-Py-5-Me)<sub>3</sub> ligand unit around its Sn–C<sub>py</sub> bond. The non-central location of the Ln atom in the cage is reflected by a bending of the Sn⋯L, n⋯Sn axis with 165.50(1)° and 167.28(13)° for Yb and Eu ions, respectively [114]. The Sn bridgehead atom of the tripod reveals a trigonal pyramidal coordination mode (Figure 3, **11b**).

The reaction of [LiSn(2-Py-5-Me)<sub>3</sub>(thf)] with [Ln(η<sup>5</sup>-C<sub>5</sub>Me<sub>5</sub>)<sub>2</sub>] precursors resulted in the formation of the first Ln<sup>II</sup> sandwich complexes, **12**, involving the anionic TPS in a κ<sup>3</sup>N-coordinating manner and featuring “naked” Sn<sup>II</sup> centers, which can be used for the following κ<sup>1</sup>Sn-metal coordination (the Eu complex is shown as an example in Figure 3, **12**) [114].

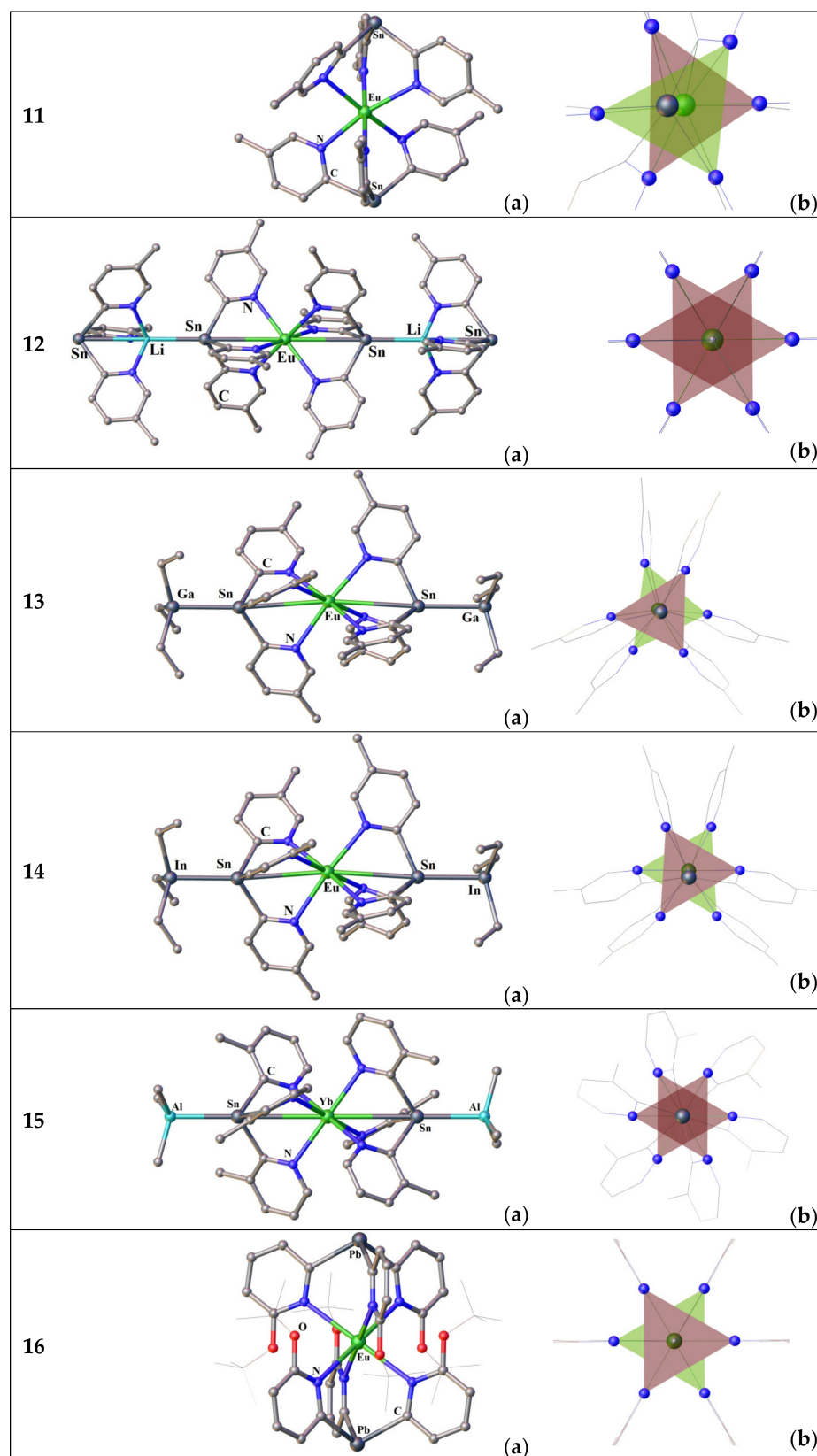


**Figure 3.** Molecular structures (a) and octahedral coordination polyhedra Ln-N<sub>6</sub>, with colored faces forming the tripod bases (b) for the compounds 11–16. Hydrogen atoms are omitted. The picture was made using open crystallographic data.

The compound **12** crystallizes in the cubic space group  $Pa\bar{3}$  with  $\text{Eu}^{2+}$  lying in a special crystallographic position and four molecules in the unit cell. The longer  $\text{Eu-N}$  (2.611(3) Å) and  $\text{Eu}\cdots\text{Sn}$  (3.8874(4) Å) distances are consistent with the larger size of the  $\text{Eu}^{2+}$  vs.  $\text{Yb}^{2+}$  cation in **11**. The most pertinent feature is the  $\text{Sn-Li}$  contact of 2.792(12) Å in **12**, which is shorter than the covalent  $\text{Sn-Li}$  bond lengths (2.831–2.897 Å) [118]. An encapsulation of the large  $\text{Eu}^{2+}$  ion and the additional  $\kappa^1\text{Sn}$  coordination of the two inner TPS ligands originate an opening of the tripodal structure ( $\text{C-Sn-C} = 99.6(1)^\circ$ ) compared to both outer TPS frameworks with the “naked” Sn centers ( $\text{C-Sn-C} = 93.6(1)^\circ$ ) [114]. Furthermore, the  $\kappa^1\text{Sn}$  binding gives a practically ideal octahedral environment of the  $\text{Eu}^{2+}$  ion with a linear  $\text{Sn}\cdots\text{Eu}\cdots\text{Sn}$  axis ( $180.0(1)^\circ$ ).

The room temperature reactions of a trialkylmetalates  $\text{MAlk}_3$  ( $\text{Alk} = \text{Me}$  for Al and Et for Ga and In) with the complex  $[\text{Ln}\{\text{Sn}(2\text{-Py-n-Me})_3\}_2]$  gave the following organometallic species:  $[\text{Eu}\{\text{Sn}(2\text{-Py-4-Me})_3\}_2\{\text{GaEt}_3\}_2]$  (**13**),  $[\text{Eu}\{\text{Sn}(2\text{-Py-4-Me})_3\}_2\{\text{InEt}_3\}_2]$  (**14**), and  $[\text{Yb}\{\text{Sn}(2\text{-Py-3-Me})_3\}_2\{\text{AlMe}_3\}_2]$  (**15**) [115]. Compounds **13** and **14** (Figure 3) have similar crystal structures and crystallize in the same space group,  $C2/c$  [115]. Eu have a distorted octahedral geometry, which is characteristic for the type **11** compounds described above. In contrast with the complexes **11**, the non-central location of the Ln ion in the coordination octahedron of **13** and **14** is much less expressed in the bending of the  $\text{Sn}\cdots\text{Eu}\cdots\text{Sn}$  axis by  $176.40(5)^\circ$  and  $172.05(8)^\circ$  for **13** and **14**, respectively. In the solid state, the complex **15** (Figure 3) reveals bonding characteristics similar to those for **13** and **14**, but differs in that the Yb ion possesses an almost perfect octahedral environment with a strictly linear  $\text{Sn}\cdots\text{Yb}\cdots\text{Sn}$  axis ( $180.0^\circ$ ) [115].

Here are a few words about the only sandwich lanthanide complex comprising tris(2-pyridyl)plumbate. The compound  $[\text{Eu}\{\text{Pb}(2\text{-Py-6-}i\text{tBu})_3\}_2]$  (**16**) has been isolated from a concentrated THF solution [117]. Like **12**, complex **16** (Figure 3) crystallizes in the  $Pa\bar{3}$  space group. The  $\text{Eu}^{2+}$  ion is coordinated by six nitrogen donor atoms of two tripods with a  $\text{Eu-N}$  bond length of 2.699(2) Å and a  $\text{Eu}\cdots\text{O}$  distance of 4.0215(1) Å, which is greater than those of 2.611(3) and 3.501(3) Å in **12**. This is because of the larger radius of the bridgehead ion in the  $\text{Pb}(2\text{-Py-6-}i\text{tBu})_3$  ligand. Although the cavity of the tripodal ligand offers an almost ideal octahedral coordination sphere for the  $\text{Eu}^{2+}$  cation, which is well encapsulated and clearly separated from the formally negatively charged Pb bridgehead atoms, compound **16** is not stable in the THF solution [117].

EPR solution studies conducted in ambient conditions for compound **16** in the presence of nitrosobenzene (NOB) have suggested the generation of a radical entity. The X-band EPR spectrum exhibits one broad signal corresponding to a  $\text{Eu}^{\text{II}} 4f^7$  spin system with a value of  $g_0 = 1.989 \pm 0.001$  and a line width of  $\Delta B_{\text{pp}} = (31.0 \pm 0.1)$  mT. An identical EPR spectrum was obtained without a spin trap. In addition to a broad signal, the spectrum shows a triplet of multiplets. The well-resolved hyperfine structure is caused by the coupling of the unpaired electron with the  $^{14}\text{N}$  ( $I = 1$ ) nucleus and three groups of non-equivalent protons of NOB. The spectrum has been well simulated, giving the values  $g_0 = 2.0057 \pm 0.0005$  and  $a_0^{\text{N}} = (1.097 \pm 0.005)$  mT, as well as  $a_0^{\text{H}} = (0.249 \pm 0.005)$  mT,  $a_0^{\text{H}} = (0.235 \pm 0.005)$  mT, and  $a_0^{\text{H}} = (0.089 \pm 0.005)$  mT, respectively [117]. The trapped radical was stable over a period of a few hours. However, no  $^{207}\text{Pb}$  hfs coupling could have been observed, indicating a radical adduct formation [117].

The complexes comprising tris(pyridyl)aluminum (TPAl) tripods are completed in this section, and their molecular structures are illustrated in Figure 4.

As was shown by R. García-Rodríguez et al. [119,120], the complexes of  $\text{Ln}^{2+}$  with TPAl are air unstable and can only be obtained by employing the sterically hindered tripods- $[(\text{Alkyl})\text{Al}(2\text{-Py-6-R})_3]^-$ , where  $\text{Alkyl} = \text{Et}$  and  $\text{R} = \text{Me}$  or  $\text{Br}$ . This means that the coordination ability of TPAl can be adjusted by the steric and electronic character of substituents in the sixth position of the pyridyls. While  $[\text{EtAl}(2\text{-py-6-Me})_3]^-$  (**17**) coordinates strongly to  $\text{Ln}^{2+}$  ions,  $[\text{EtAl}(2\text{-py-6-Br})_3]^-$  (**18**) forms much weaker complexes, and  $[\text{EtAl}(2\text{-py-6-CF}_3)_3]^-$  does not coordinate at all [120]. Synthetic and structural investigations were essentially devoted to the complexes of two anions— $[\text{EtAl}(2\text{-Py-6-Me})_3]^-$  and

$[\text{EtAl}(\text{2-Py-6-Br})_3]^-$ . The 2:1 ratio reactions of the compound **17** with  $\text{LnI}_2$  ( $\text{Ln} = \text{Eu}, \text{Yb}$ , and  $\text{Sm}$ ) in thf at room temperature led to the formation of the deep-orange (Eu) or purple (Yb and Sm) solutions after 24 h, which indicates Ln coordination [119,120]. The SC-XRD study confirmed the formation of sandwich complexes:  $[\{\text{Ln}(\text{EtAl}(\text{2-py-6-Me})_3)_2\}]$  ( $\text{Ln} = \text{Sm}$  **18**,  $\text{Eu}$  **19**, and  $\text{Yb}$  **20**) and  $[\{\text{Eu}(\text{EtAl}(\text{2-py-6-Br})_3)_2\}]$  (**21**); see Figure 4. The complexes **18** and **21** crystallize in the  $P\bar{1}$  space group. The first contains one  $\text{CH}_3\text{C}_6\text{H}_5$  molecule as a solvate upon crystallizing from toluene. The coordination environments formed around Sm or Eu are a slightly elongated octahedron and a trigonal antiprism, respectively, although both compounds have a straight line passing through the bridgehead atoms of the tripods (for Al–Ln–Al, the angle is  $180^\circ$ ). The compounds **19** and **20** crystallize in the  $P4_32_12$  and  $P2_1/n$  space groups, respectively. The molecules of **19** and **20** feature six-coordinate, distorted, octahedral lanthanide ions, with the N–Ln–N angles being approximately  $90^\circ$  and a slightly bent Al–Ln–Al axis ( $177.17^\circ$  (**19**) and  $178.23^\circ$  (**20**)) [120].

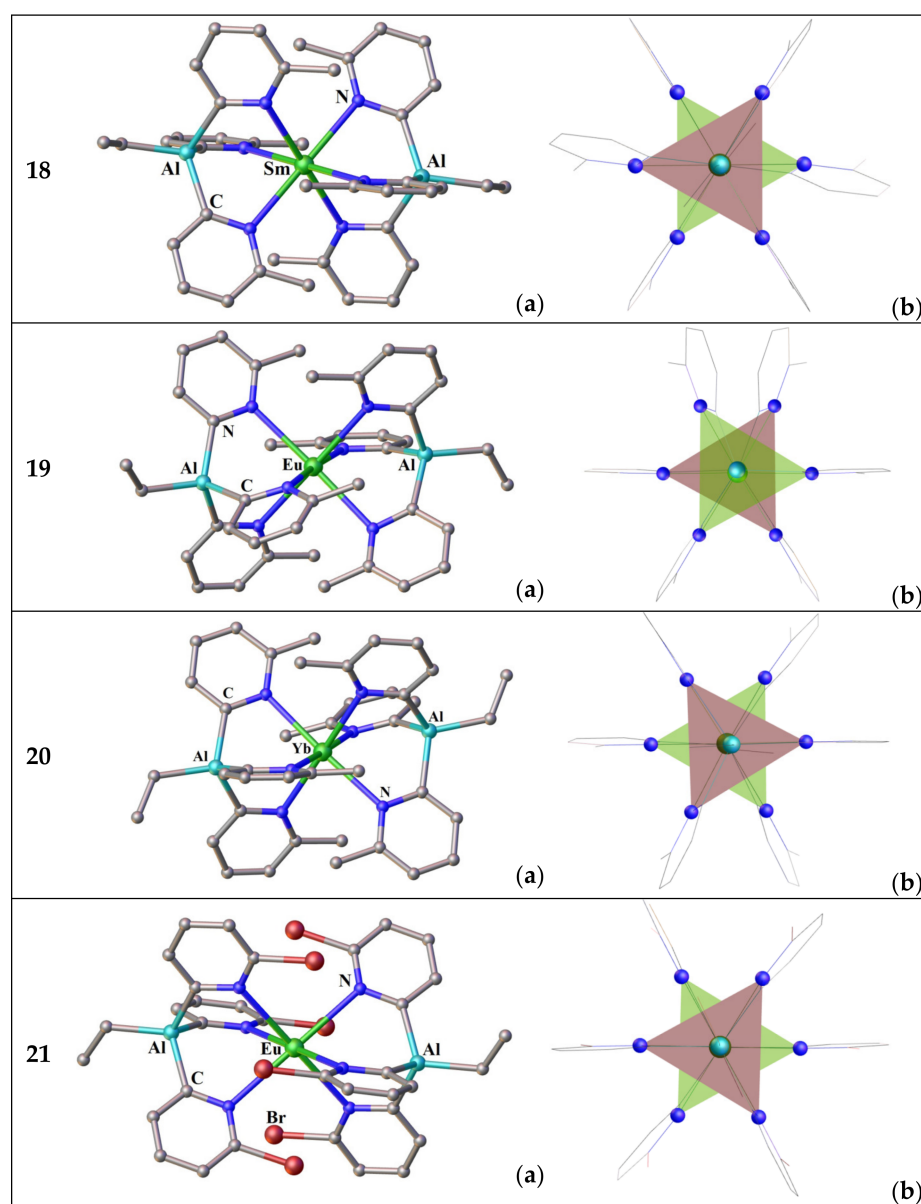


**Figure 4.** Molecular structures (a) and coordination polyhedra  $\text{Ln-N}_6$ , with colored faces forming the tripod bases (b) for the compounds **18–21**. Hydrogen atoms are omitted. The picture was made using open crystallographic data.

None of the Ln compounds comprising tris(2-pyridyl)metalates have been reported for their magnetic behavior. The next fairly representative group of lanthanide compounds with tripodal ligands are complexes with tris(2-pyridyl)amines.

### 3.2.2. Complexes of Tris(2-Pyridyl)Amines

The interaction of tris(2-pyridylmethyl)amine (TPA) with the precursors  $\text{LnHal}_3(\text{thf})_4$  or  $\text{Ln}(\text{OTf})_3$  was investigated in an anhydrous environment and in the presence of water [3,7]. In the absence of water, the succeeding formation of both mono- and bis-(TPA) was detected using a lanthanide/ligand ratio of 1 and 2, respectively. The mono-TPA complexes  $[\text{Ce}(\text{TPA})\text{I}_3]$  (**22**) [3],  $[\text{Ln}(\text{TPA})\text{Cl}_3]$  (Ln(III) = Eu, Tb, and Lu ([7]), and the bis(tpa) complexes  $[\text{Ln}(\text{TPA})_2]\text{X}_3$  (X = I,  $\text{Ln}^{3+}$  = La, Ce, Nd, Lu [3], and Sm [6]; X = OTf), bis(tpa) complexes  $[\text{Ln}(\text{TPA})_2]\text{X}_3$  (X = I,  $\text{Ln}^{3+}$  = La, Ce, Nd, Lu [3], and Sm [6]; X = OTf, Eu [3]) were obtained under anhydrous conditions, and their crystal structures were determined.

The complexes  $[\text{Ln}(\text{TPA})\text{Hal}_3]$  (see, as an example the Ce complex (**22**) in Figure 5) are isomorphous, and they crystallize in the space group  $P2_1/c$  without any solvent molecules per each crystal cell. Note that a tripod base and a plane passing through the halide ions are not parallel. The monotripod complexes  $[\text{Ln}(\text{TPA})\text{Cl}_3(\text{CH}_3\text{OH})]\cdot\text{CH}_3\text{OH}$  (**23**) ( $\text{Ln}^{3+}$  = La, Nd, and Sm) (Figure 5) were also obtained starting from the corresponding hydrated lanthanide halide  $[\text{LnCl}_3(\text{H}_2\text{O})_6]$  [121]. Nonetheless, the compounds in **23** are not of interest as high-performance SMMs because they do not have monoaxiality.

In contrast, the heteroleptic complexes containing three nitrates and one tripodal tetradentate ligand tris((1*H*-pyrazol-1-yl)methyl)amine (TPzMA) are enough axial (Figure 5, **23a**) [12]. Their synthesis, structure, and photophysical and magnetic properties of sequence complexes  $[\text{Ln}(\text{TPzMA})(\text{NO}_3)_3]\cdot n\text{MeCN}$  (Ln = Eu, Tb, Dy, and Er,  $n = 0.5$ ; Yb,  $n = 0$ ) were described [12]. The SCXRD analysis reveals that, among the investigated compounds, the compounds of Eu, Tb, Dy, and Er are isomorphous and crystallize in the triclinic  $P\bar{1}$  space group with a single complex molecule and 1/2 of a  $\text{CH}_3\text{CN}$  molecule per asymmetric unit. The structure includes a mononuclear complex in which the  $\text{Ln}^{3+}$  ion is coordinated by four N atoms from the TPzMA ligand and six oxygen atoms belonging to the three bidentate nitrate anions (Figure 5, **23a**). The tripodal ligand is coordinated by the central ion in a symmetrical manner, forming the  $\text{Ln}^{3+}$  coordination polyhedron together with nitrates, which is better described as a distorted spherocorona [12]. Contrary to its congeners, the Yb complex crystallizes in the monoclinic  $P2_1/c$  space group without solvates. Probably, due to the Ln contraction and the fall in intramolecular distances resulting in steric repulsions in the polyhedron, only two nitrate moieties are bidentate and the other one is monodentate, which leads to a muffin geometry of the Yb site with  $C_s$  symmetry [12].

The europium, terbium, and dysprosium analogues exhibit a lanthanide-based luminescence, while the dysprosium, erbium, and ytterbium compounds show field-induced slow relaxation of their magnetization involving Raman and direct processes.

The complexes  $[\text{Ln}(\text{TPA})_2]\text{I}_3\cdot\text{CH}_3\text{CN}$  (Ln = La, Ce, Nd, and Sm) are isostructural to each other (Figure 5, **24**) [3,6]. The metal ions are eight-coordinated by the two-tetradentate ligands that wrap around the metal in a pseudo- $D_3$  symmetric arrangement [3]. All the complexes crystallize as a single enantiomer in the non-centrosymmetric space group  $P2_12_12_1$  [3]. The coordination polyhedra are best defined as distorted cubes with a less distorted geometry for Lu [3].

It was not possible to obtain the crystal structure of  $[\text{Eu}(\text{TPA})_2]\cdot 3\text{OTf}$  under water-free conditions. The single crystals of  $[\text{Eu}(\text{TPA})_2]\cdot 3\text{OTf}\cdot\text{CH}_3\text{CN}\cdot 0.3\text{H}_2\text{O}$  (**25**) were obtained in the presence of a  $\sim 0.5$  equivalent of  $\text{H}_2\text{O}$ . The molecular structure of **25** (Figure 5, **25**) is very close to that of the Ln-bis(tpa) iodides. Contrary to the complexes of **24**, complex **25** crystallizes in the centrosymmetric space group  $P2_1/c$  with two complex molecules per asymmetric unit and a 0.15 molecule of  $\text{H}_2\text{O}$ , which apparently helps with the crystallization [3].

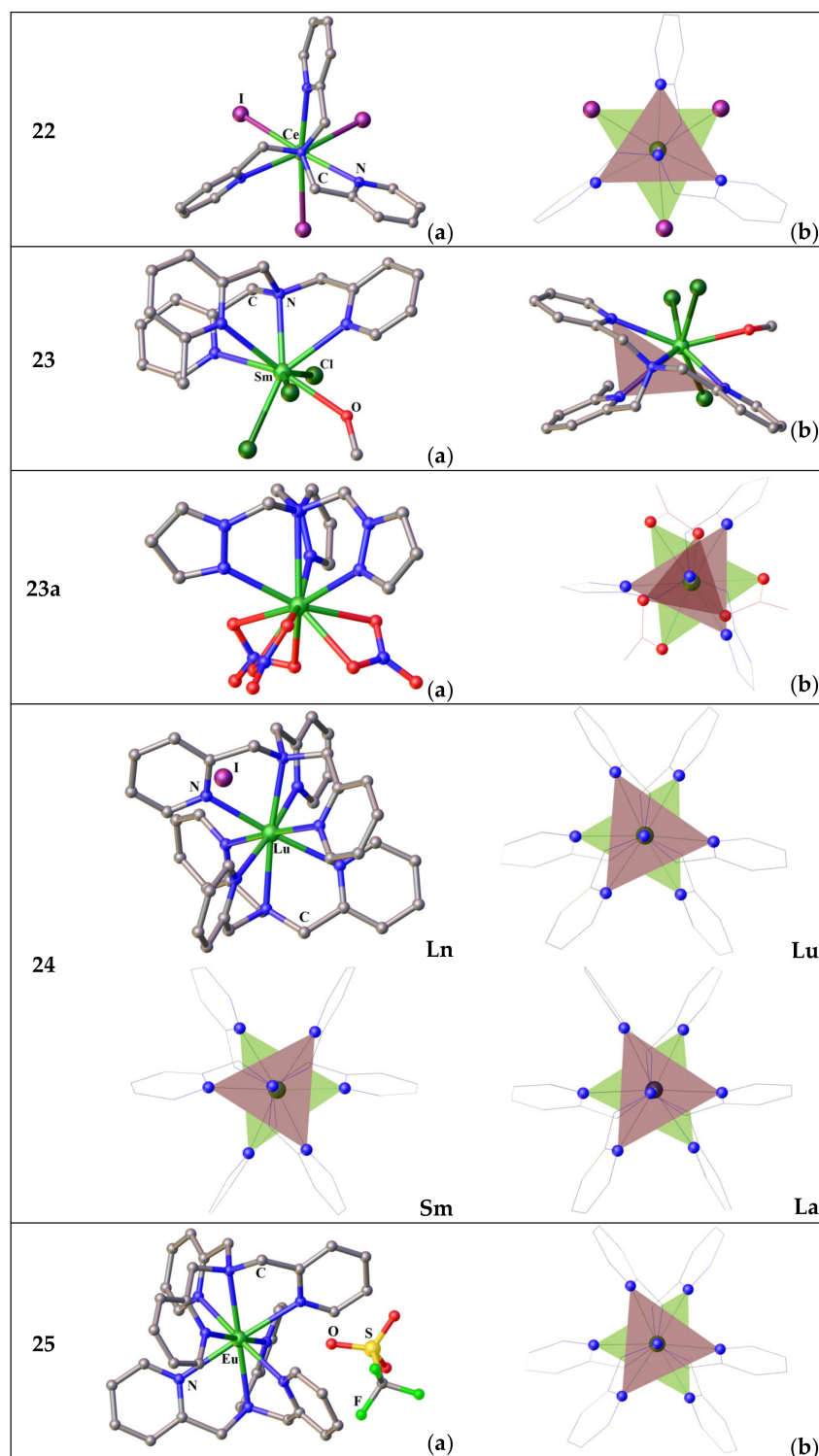


**Figure 5.** Molecular structures (left) and coordination polyhedra Ln-N<sub>6</sub>, with colored faces forming the tripod bases (right) for the compounds 22–25. Hydrogen atoms are omitted. The picture was made using open crystallographic data.

Along with the Ln<sup>3+</sup> TPA complexes, their congeners of Ln<sup>2+</sup> were also isolated. Starting from LnI<sub>2</sub>, the stable mono- and bis-TPA complexes [Yb(TPA)I<sub>2</sub>(MeCN)]·MeCN (26) (Figure 6, 26) and [Ln(TPA)I<sub>2</sub>] (Ln<sup>2+</sup> = Sm and Eu) (27), [Ln(TPA)<sub>2</sub>]·2I·0.5MeCN (Ln<sup>2+</sup> = Sm and Yb) (28) (Figure 6, 28) were prepared and characterized [6]. When the bulk anion NaBPh<sub>4</sub> is added to the previous reaction mixture, a number of compounds

with TPA and its methyl analogs were obtained in inert conditions [122]. The compounds  $[\text{Ln}(\text{Me}_n\text{TPA})_2](\text{BPh}_4)_2$  ( $n = 0-3$  reliant on the methylation degree of the six positions of the pyridyl rings of  $\text{Me}_n\text{TPA}$ , when  $n = 0$ — $\text{Ln}^{2+} = \text{Eu}, \text{Yb}$  **29** (Figure 6, **29**);  $n = 2$ — $\text{Ln}^{2+} = \text{Eu}, \text{Yb}$  (**30**); and  $n = 3$ — $\text{Ln}^{2+} = \text{Eu}$  (**31**) (Figure 6, **31**)) have been synthesized, and their structural, electrochemical, and photophysical properties have been studied [122].

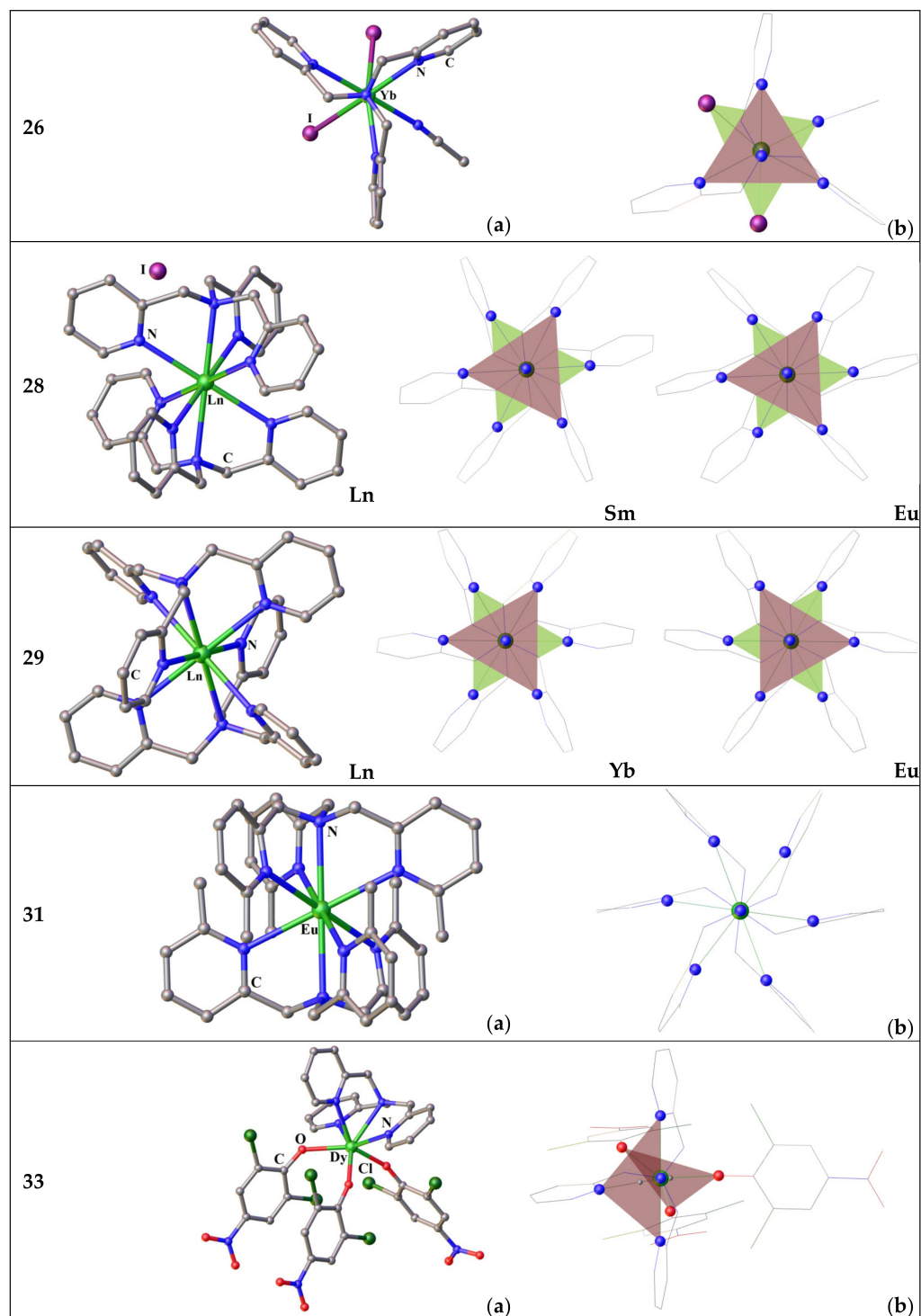


**Figure 6.** Molecular structures (left) and coordination polyhedra  $\text{Ln-N}_6$ , with colored faces forming the tripod bases (right) for the compounds **26–33**. Hydrogen atoms are omitted. The picture was made using open crystallographic data.

The complexes **27**  $[\text{Ln}(\text{TPA})_2] \cdot 2\text{I}$  crystallize in the monoclinic centrosymmetric  $P2_1/c$  space group, while the complexes **28**  $[\text{Ln}(\text{TPA})_2] \cdot 2\text{I} \cdot 0.5\text{CH}_3\text{CN}$  crystallize in the non-centrosymmetric monoclinic  $Cc$  space group [6]. The complexes **29** crystallize in the monoclinic  $P2_1/n$  space group, contrary to **30** and **31**, which crystallize in the triclinic  $P\bar{1}$  space group, with the lowering of symmetry attributed to the presence of the methyl substituents that result in a crystallographic disorder [122]. The  $\text{Ln}^{2+}$  ion is eight-coordinated in all the sandwich compounds. Continuous shape measures using the software SHAPE 2.1 were employed to determine the geometry of the Ln centers and suggest that the coordination geometry is closest to cubic in all cases [122]. The shape distortion parameters are in the range 0.69–1.53 for the cubic geometry; the further the value is from zero, the greater the distortion from the ideal geometry [122].

Unfortunately, for all the above compounds comprising the TPA ligand (both for sandwich and semisandwich), the magnetic properties have not been studied. Only two  $[\text{Ln}(\text{TPA})(\text{Anion})_3]$  compounds and four  $[\text{Ln}(\text{TPzMA})(\text{NO}_3)_3] \cdot \text{complexes}$  have been magnetically characterized [123]. The description of their magnetic behavior concludes the current section of the review.

The two mononuclear seven-coordinated  $\text{Dy}^{3+}$  complexes— $[\text{Dy}(\text{TPA})\text{Cl}_3]$  (**32**) and  $[\text{Dy}(\text{TPA})(\text{OphCl}_2\text{NO}_2)_3] \cdot 0.5\text{CH}_2\text{Cl}_2$  (**33**) have been synthesized using the neutral TPA ligand and either the strong ligand 2,6-dichloro-4-nitrophenol ( $\text{Cl}_2\text{NO}_2\text{PhOH}$ ) or the weak ligand field donor  $\text{Cl}^-$  [123]. As in the tri-iodine compounds of type **22**, mentioned above, the  $\text{Dy}^{3+}$  ions in complexes **32** and **33** have seven-coordinated capped octahedral and capped trigonal prismatic coordination geometries, respectively [123]. Magnetic studies have shown that both Dy compounds possess field-induced slow magnetic relaxation. The energy barrier for **33** is higher than that of **32**, which is due to the strong ligand field of  $\text{Cl}_2\text{NO}_2\text{PhO}^-$  vs.  $\text{Cl}^-$ , resulting in a larger magnetic anisotropy of **33** compared to **32** [123]. The direction of the magnetic anisotropy axes in both complexes deviates remarkably from the symmetry axis of the capped octahedron ( $C_{3v}$ ) and the capped trigonal prismatic ( $C_{2v}$ ), which explains the poor performance of the SIM behavior for both complexes [123].

The room-temperature  $\chi T$  values of 12.97, 13.92, 11.54, and 3.20 emu/mol for **23a**, respectively, for  $[\text{Ln}(\text{TpzMA})(\text{NO}_3)_3] \cdot (\text{Ln} = \text{Tb}, \text{Dy}, \text{Er}, \text{and } \text{Yb})$ , are in quite good accordance with the theoretical values of 11.82, 14.17, 11.48, and 2.57 emu/mol estimated for a unique  $\text{Ln}^{3+}$  ion [12]. Upon cooling, all the compounds exhibit the typical decrease in  $\chi T$  caused by the thermal depopulation of the  $m_j$  levels, reaching values at 1.8 K of 5.25 and 7.35 [12]. For all the complexes, the absence of saturation for the magnetization curves testifies to the existence of magnetic anisotropy, which is expected for such lanthanide ions [12]. Under a zero dc field, no strong out-of-phase susceptibility ( $\chi''$ ) components were observed for any of the samples, pointing out the occurrence of fast QTM.

Excluding the Tb complex, for which the out-of-phase component remains weak, all other complexes show a strong  $\chi''$  component upon applying the dc field. For the Er and Yb compounds, the appearance of a second low-frequency peak was detected at high magnetic fields. This might originate from different relaxation mechanisms actuated by large magnetic fields [12]. Therefore, it appears that the neutral tetradentate TPzMA ligand in association with nitrates and the resulting low symmetry of the lanthanide site do not provide the requirements to maximize the anisotropy for either oblate or prolate lanthanide ions in the zero dc field [12].

#### 4. Complexes with Paramagnetic Ligands

Metal-radical systems are recognized to display better SMM characteristics [124]. For example, an extra unpaired electron transforms  $(n\text{-Bu})_4\text{N}[\text{TbPc}_2]$  (Pc is a dianion of phthalocyanine) into  $[\text{TbPc}_2]$  (Kramers system), guaranteeing twofold degeneracy of all electronic levels enforced by time reversal symmetry, irrespective of ligand field symmetry [125]. Park et al. [126] stated that higher energy levels strongly depend on the ligand type, molecular symmetry, and overall charge of the molecule. Additionally, ligand distortion and molecular symmetry significantly affect the transverse CF parameters, leading to tunnel

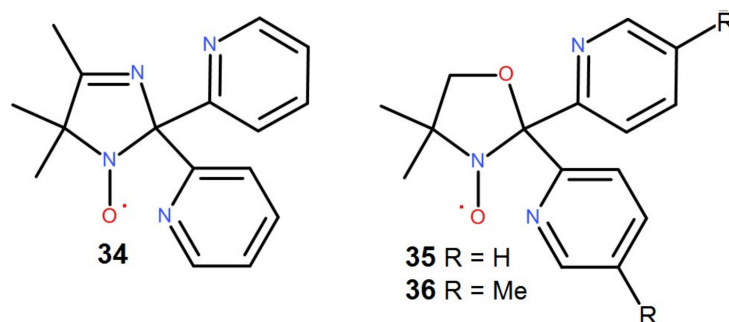
splitting. The latter induces QTM. Compared to the anionic complex  $[\text{TbPc}_2]^-$ , for the neutral complex, no tunnel splitting was observed for the ground and excited state quasi-doublets [126]. For the anionic complex, tunnel splittings of 0.007, 0.090, and  $7.969\text{ cm}^{-1}$  were observed for the ground, first, and second excited state quasi-doublets. The perceived dissimilarity in the magnetic behavior was attributed to the significant exchange interaction,  $J_{ex}$  of  $\sim 7\text{ cm}^{-1}$ , existing in the compound  $[\text{TbPc}_2]$  compared to the anionic one [126]. Moreover, the axial CF parameter ( $B_2^0 = -5.93$  vs.  $-5.05\text{ cm}^{-1}$ ) is larger, and the transverse CF parameter ( $B_2^2 = 0.3$  to  $0.4\text{ cm}^{-1}$  vs.  $0.8$  to  $3.6\text{ cm}^{-1}$ ) is small for the latter [126].

The real influence of exchange coupling on magnetic relaxation dynamics was reported by Long et al., who first described the Ln complexes with large  $T_B$  values [127]. They obtained a binuclear  $\text{Tb}^{3+}$  complex  $[\{[(\text{Me}_3\text{Si})_2\text{N}]_2(\text{THF})\text{Tb}\}_2(\mu\text{-}\eta^2\text{-}\eta^2\text{-N}_2)^-]$  (**TbN<sub>2</sub>Tb**), in which a large magnetic interaction between  $\text{Tb}^{3+}$  and the radical was established to quench QTM in the absence of a magnetic field. This SMM relaxed in the thermally activated direct process with (QTM probability  $B \sim 10^{-6}$ ) a  $U_{eff} = 227\text{ cm}^{-1}$  and  $T_B \sim 14\text{ K}$  [127]. Later, the strong coupling of  $-27\text{ cm}^{-1}$  was communicated for the Gd congener of **TbN<sub>2</sub>Tb** [128]. For the **GdN<sub>2</sub>Gd**, electronic structure calculations were performed, which clearly demonstrated a direct overlap between the  $\text{Gd}^{3+}$  4f orbitals and the  $\pi^*$  orbital of the radical [129].

#### 4.1. Complexes of the Tripodal Nitroxyl Radicals

##### 4.1.1. Functionalized by 2-Pyridyl Groups Paramagnetic Tripods and Their Complexes

The stable nitroxyl radicals are widely used in the field of molecular magnetism [130–135]. However, till now, only three tripodal nitroxyl radicals functionalized by pyridyl groups (Scheme 1) are known [25,136]. The complexes of 3D metal ions with the radical tripods **34–36** are mostly sandwich types [25–32,137]), while a number of semisandwich Ln complexes (**37**) have recently been synthesized [138,139] (Figure 7). In contrast to the tetradentate TPA tripods described above, the tripodal oxazolidine radical (Rad) **35** is sterically rigid. Upon coordination, it forms a pyramid with an almost ideal triangle at the face for both monoradical (**37**) and biradical complexes (**38**) (Figure 7) [138,140].



**Scheme 1.** 2,5-Dihydro-4,5,5-Trimethyl-2,2-Bis(2-Pyridyl)Imidazole-1-Oxyl, **34**; 4,4-dimethyl-2,2-di(2-pyridyl) oxazolidine-N-oxyl, **35**; and 4,4-dimethyl-2,2-bis [2-(4-methylpyridyl)]oxazolidine-N-oxyl, **36**—radical tripods.

##### 4.1.2. Structural Features of the Paramagnetic Tripod Complexes

According to the PRXD study, monoradical complexes  $[\text{LnRad}(\text{NO}_3)_3]$  (**37**) are isostructural. The crystal structures for the complexes of  $\text{Ln}^{3+} = \text{Dy}, \text{Tm}, \text{Y}, \text{Eu},$  and  $\text{Lu}$  are ascertained by SC-RXD experiments. Like their closest relatives, the nitrate complexes of Ln with the diamagnetic tripod TPM (**9**) and the compounds **37** crystallize in the non-centrosymmetric  $P2_1/n$  space group [138]. In these complexes, Rad coordinates to a Ln ion in a tridentate manner via two N atoms of the pyridyl substituents and an O atom of an NO group. The coordination sphere is further complemented by three bidentate nitrates to give an  $\text{LnO}_7\text{N}_2$  polyhedron [138]. Consistent with the continuous symmetry measures method [104], the polyhedron is best described as a spherical tricapped trigonal prism. The radical donor atoms compose the triangular face of the prism. In addition, the

coordinated oxygen atoms of the nitrate ligands also form triangular planes parallel to those of Rad (Figure 7, 37b). Moreover, the centers of all the triangles lie on the same axis passing through a central Ln atom, which bears witness to  $S_3$  symmetry.

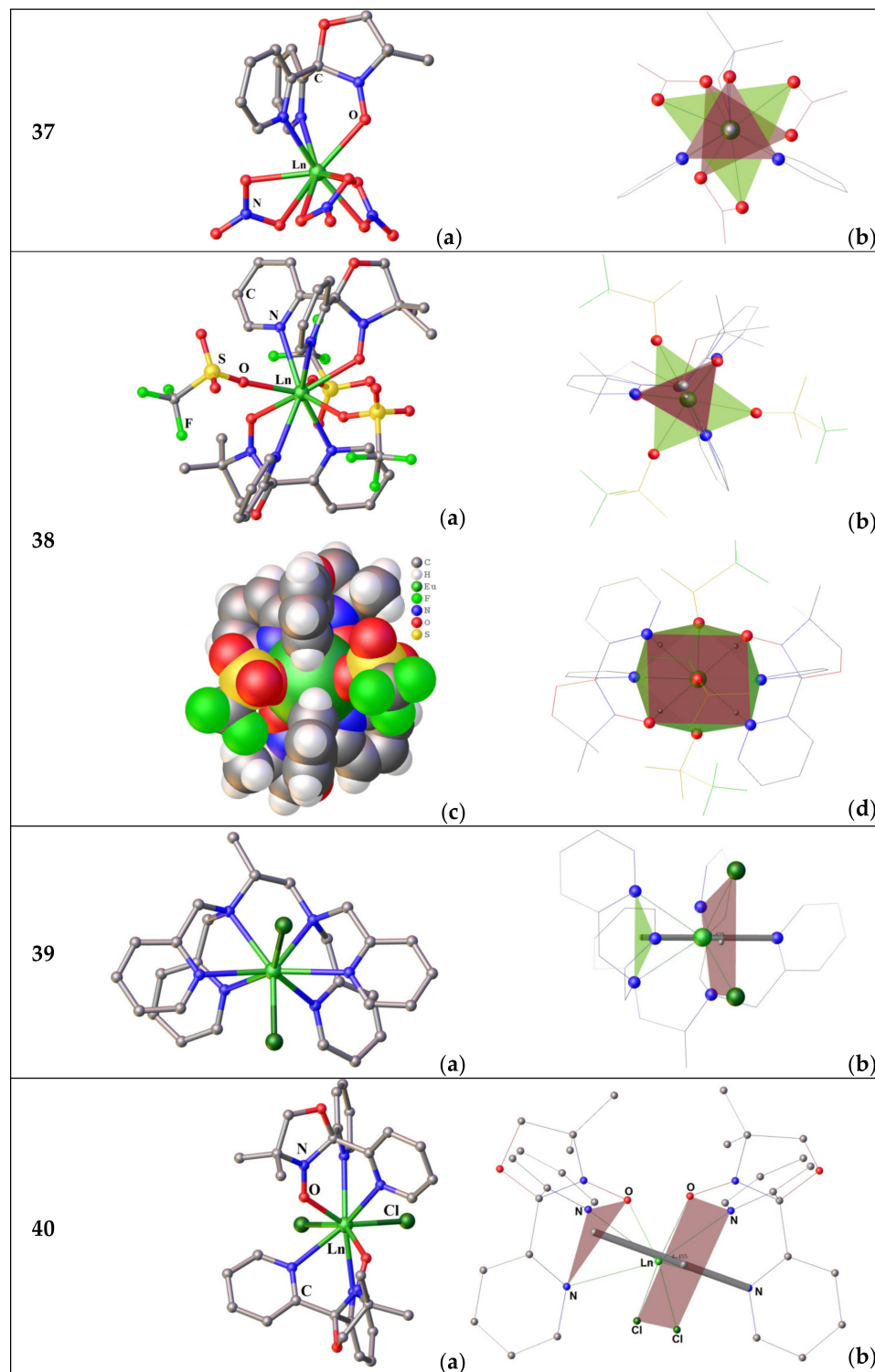


**Figure 7.** Molecular structures (a) and coordination Ln polyhedra with colored planes forming the tripod bases (b) for the compounds 37–39. Hydrogen atoms are omitted. The picture was made using open crystallographic data.

The Ln–O bond distances related to the NO moiety vary in a region of 2.34–2.38 Å. The length of the N–O bonds of the nitroxyl group fluctuate in the 1.25–1.28 Å interval. Markedly, all bond lengths and angles of the complexes are in the expected range [138]. The Ln environment is composed of three monodentate anions to give the LnO<sub>5</sub>N<sub>4</sub> polyhedron. Unlike nitrate ligands, triflate is bound to Ln only by one donor O atom, and the three CF<sub>3</sub>SO<sub>3</sub> ions are located in the equatorial plane of the compounds **38**. At first glance, the latter have *D*<sub>3h</sub> pseudo-symmetry since the tripod bases are placed one above the other and the three O atoms from the anionic ligands form a triangle (Figure 7, **38b**). However, due to the “sandwich” bending, all the triangles are distorted. The SHAPE analysis [104] gave the polyhedron geometry (Figure 7, **38d**) as a spherical capped square antiprism with the point symmetry close to *C*<sub>4v</sub> [140]. It should be noted that the radical’s donor atoms and the two oxygens belonging to the two triflate ligands compose the faces of the antiprism, while an oxygen of the third triflate arranges above the rectangular face (Figure 7, **38b**) [140].

The only two related compounds of complex **38** are the Ln<sup>3+</sup> complexes with a quasi-tripodal ligand, 1,3,5-trimethyl-triazacyclohexane (Me<sub>3</sub>tach), [Pr(Me<sub>3</sub>tach)<sub>2</sub>(OTf)<sub>3</sub>] [141], and HMe<sub>3</sub>tach[La(Me<sub>3</sub>tach)<sub>2</sub>(OTf)<sub>4</sub>] [142] (Figure 8). The former is so bent that the three triflates are not evenly distributed in the equatorial plane, while the latter is even capable of housing four triflates. Such a geometrical organization of the Ln coordination sphere is favorable to stabilize the highest *m<sub>J</sub>* ground states for the prolate tripositive lanthanides ions (Pm, Sm, Er, Tm, and Yb). That is why the Dy complex **38**, studied by us earlier, does not exhibit slow magnetic relaxation. The most attractive geometry (for prolate-type Ln<sup>3+</sup>) among compounds with this pseudo-tripodal ligand has recently been studied. The only non-bent sandwich complex [La(Me<sub>3</sub>tach)<sub>2</sub>Cl<sub>3</sub>] with three chlorine anionic ligands in an equatorial plane is presented in Figure 9 [142]. However, chloride anions are bulky enough to enter all three of the inner spheres of smaller Ln<sup>3+</sup> ions, starting with samarium. Nevertheless, the two chlorides can fit quite well in the equatorial plane of the Ln coordination sphere. However, we did not find an example of such a species for any [Ln(tripod)<sub>2</sub>Cl<sub>2</sub>]<sup>+</sup>.

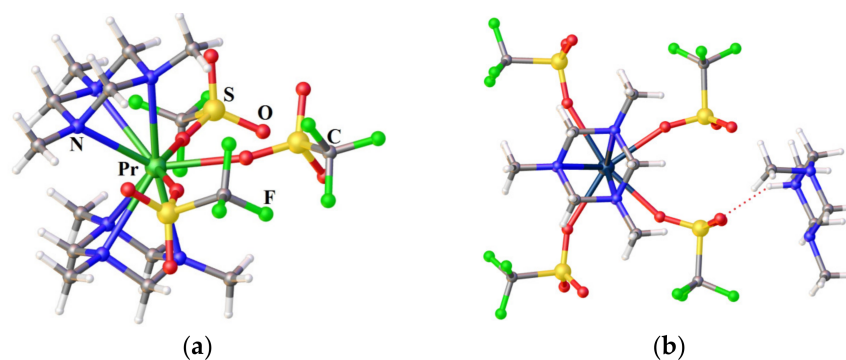


**Figure 8.** (a) Tri-triflate complex [Pr(Me<sub>3</sub>tach)<sub>2</sub>(OTf)<sub>3</sub>] [141]. (b) Four-triflate complex HMe<sub>3</sub>tach[La(Me<sub>3</sub>tach)<sub>2</sub>(OTf)<sub>4</sub>] [142] complexes. The picture was made using open crystallographic data.

According to the CCDC database, there are only a few examples of such compounds with bis-tripodal ligands. One of them is the Eu<sup>3+</sup> complex [Eu<sup>III</sup>Cl<sub>2</sub>(R)-tppn]ClO<sub>4</sub> (**39**) [143], Figure 7. The coordination geometry of **39** is best described as a distorted dodecahedron. The authors point out that the four coordinated pyridyl nitrogens and one from the two chlorine atoms are approximately located on a plane and form a pentagon, the other Cl being coordinated almost perpendicular to this plane. However, from our point of view, it is better to choose a different description of the geometry for compound **39** in order to predict its magnetic behavior. Both Cl anions are best placed in the same plane, as shown in Figure 7, **39b**. In this case, the molecule have an axis, which could serve as an axis of magnetic anisotropy. Our preliminary studies have shown that sandwich-type complexes containing two chloride ligands in the equatorial plane of the cationic complex **40** (Figure 7) can also be obtained for the paramagnetic tripod **35** [144].

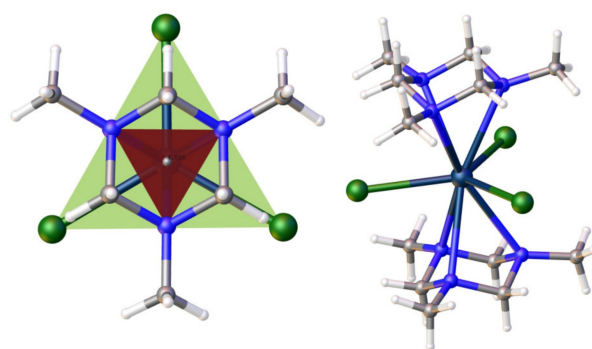


**Figure 9.** The compound  $[\text{La}(\text{Me}_3\text{tach})_2\text{Cl}_3]$  with three chlorine anionic ligands in equatorial plane. The picture was made using open crystallographic data.

#### 4.1.3. Magnetic Properties of the Paramagnetic Tripod Complexes

At 300 K, the  $\chi T$  product values are 7.814, 12.210, 14.366, and 7.376 emu K/mol for the 37-type compounds of Gd, Tb, Dy, and Tm, respectively. These values are consistent with the expected ones for the appropriate  $\text{Ln}^{\text{III}}$  ion plus a radical (8.255, 12.195, 14.545, and 7.525 emu K/mol) [138]. With the temperature lowering, the  $\chi T$  value for all the complexes drops considerably, which can be ascribed to CFS and/or the antiferromagnetic metal-radical interaction. A dominance of the CFS for all Ln except Gd could be assumed, which is magnetically isotropic at the first order. It should be emphasized that the 37-Tm complex, for which the non-magnetic  $m_j = 0$ , ground state is stabilized ( $\chi T$  is equal to 0.375 emu K/mol, corresponding to the value of a radical tripod). Furthermore, the important decrease in  $\chi T$  for 37-Gd bears witness to a strong antiferromagnetic (AFM) coupling between the  $\text{Gd}^{\text{III}}$  ion and the radical. The plot  $M(H)$  for the 37-Gd complex is very informative. Considering the low crystal field splitting typical of  $\text{Gd}^{3+}$ , the saturation value of 6  $\mu_B$  is consistent with an AFM coupling between a spin  $S = 7/2$  and a radical spin  $S = \frac{1}{2}$  ( $S_{\text{tot}} = 7/2 - 1/2 = 3$ ) [138]. An X-band EPR study was performed on  $[\text{GdRad}(\text{NO}_3)_3]$  in order to obtain precise information about the electronic structure. The spectrum of Gd exhibits several broad transitions. A satisfactory fitting of both the EPR and the static magnetic measurements can be obtained using the following Hamiltonian [138]:

$$\mathcal{H} = b_2^0 \hat{O}_2^0 + b_2^2 \hat{O}_2^2 + b_4^0 \hat{O}_4^0 + j \hat{S}_{\text{Gd}} \cdot \hat{S}_{\text{rad}} + g_{\text{Gd}} \mu_B \hat{S}_{\text{Gd}} \cdot B + g_{\text{rad}} \mu_B \hat{S}_{\text{rad}} \cdot B$$

where the first three terms parametrize the CFS of the  $\text{Gd}^{\text{III}}$  ion, the fourth term is the isotropic magnetic coupling between Gd and the radical, and the last two terms are the Zeeman splitting for Gd and the radical, respectively. The finest simulation result was achieved with the values  $b_2^0 = 5.2 \times 10^{-2} \text{ cm}^{-1}$ ,  $b_2^2 = 1.1 \times 10^{-2} \text{ cm}^{-1}$ ,  $b_4^0 = 3.8 \times 10^{-4} \text{ cm}^{-1}$ ,  $j = +23 \text{ cm}^{-1}$ ,  $g_{\text{Gd}} = 2.0023$ , and  $g_{\text{rad}} = 1.998$ . Notably, the value of  $+23 \text{ cm}^{-1}$  of the isotropic coupling constant is unusually large for gadolinium complexes of organic radicals. For example, for  $\text{Gd}^{3+}$  hexafluoroacetylacetonate complexes containing one acyclic nitroxyl radical [145–147], the  $|j|$  value fluctuates between 9.6 and  $12.5 \text{ cm}^{-1}$ . For the similar compounds, including one nitronyl nitroxyl radical [148–153], exchange coupling is also inferior ( $|j| = 0.77 \div 8.35 \text{ cm}^{-1}$ ). For the Gd complex comprising the congener of Rad TEMPO (TEMPO = 2,2,6,6-tetramethylpiperidin-1-oxyl), the metal–radical interaction is very small ( $j = 2.43 \text{ cm}^{-1}$ ) [154]. For the monosemiquinone complex  $[\text{Gd}(\text{HBTp}_3)_2\text{SQ}]$ ,  $j$  is equal  $11.4 \text{ cm}^{-1}$  [155]. Moreover, the exchange interaction strength for the Gd radical in the  $[\text{GdRad}(\text{NO}_3)_3]$  species is comparable with that of the binuclear Gd complex of the purely inorganic single radical  $\text{N}_2^{3-}$  obtained in the group of J. Long [128]. The origin of such a strong magnetic exchange interaction in 37 must be ascribed to a favorable metal-to-ligand orbital superposition. In contrast to the most studied complexes with nitronyl and imino nitroxyl radicals, in which the spin density is mainly delocalized over four or three centers (O–N... N–O [156], and N... N–O), in 37, an unpaired electron is shared only between two sites. Consequently, the spin density on the donor oxygen atom in Rad is two times

higher than that in the nitronyl nitroxyl radicals. Notably, the exchange interaction is directly related to magnetic orbital overlapping, which depends on the symmetry and donor strength of all ligands [138].

The dynamic magnetic studies were carried out to gather information on magnetization dynamics at low temperatures. A frequency scan at various applied fields for **37** was performed at a temperature of 2 K. The only compound to display a relevant non-zero out-of-phase magnetic susceptibility was **37-Tb**. The latter displays slow relaxation, both with and without an externally applied field. In a zero applied field, the relaxation of **37-Tb** at 2 K was at the upper edge of accessible frequencies with a relaxation time of ca. 16  $\mu$ s; for this reason, a temperature study was impossible. When an external magnetic field was applied, the slow relaxation of **37-Tb** slowed by several orders of magnitude [138]. The relaxation time best fit was obtained using a combination of quantum tunneling and Orbach processes, giving  $\tau_{QT} = 12(1)$  ms,  $\tau_0 = 0.9(3)$  ns, and  $\Delta E = 57$   $\text{cm}^{-1}$  [138].

The magnetic studies on powder samples of the biradical complex **38** were also fulfilled. The  $\chi_m T$ -value at 300 K for the **38-Dy** compound (14.735 emu K/mol) was slightly smaller than the theoretical one (14.92 emu K/mol) for the non-interacting two radicals and one  $\text{Dy}^{3+}$  ion ( $S = 1/2$ ,  $g = 2.0023$ , and 0.375 emu K/mol) ( $4f^9$ ,  $S = 5/2$ ,  $L = 5$ ,  $J = 15/2$ ,  $g_J = 4/3$ ,  ${}^6\text{H}_{15/2}$ , 14.17 emu K/mol). However, this value corresponds well to those of 14.365 emu K/mol, which were previously obtained for the monoradical complex **37-Dy** [138], taking into account the fact that the experimental values for  $\text{Dy}^{3+}$  in a related coordination environment are somewhat lower than those for a free ion: 13.92–14.00 [12,157]. On cooling, the  $\chi_m T$  value remains almost unchanged up to 90 K, then steadily falls down to 10 emu K  $\text{mol}^{-1}$  at 20 K, and finally drops to 4.803 emu K  $\text{mol}^{-1}$  at 2 K. The latter is considerably lower than that for the monoradical analogue (6.50 emu K/mol). Since significant intermolecular exchange interactions in **38-Dy** can be excluded, the cause of such behavior could be attributed to the radical–radical coupling, which can reach high values ( $J_{\text{TEMPO1-TEMPO2}}/k_B = -24.9$  K) in  $[\text{Y}(\text{hfac})_3(\text{TEMPO})_2]$  [158]. Moreover, the metal-to-radical coupling in the  $[\text{Gd}(\text{hfac})_3(\text{TEMPO})_2]$  complex has been reported to be either positive or negative for the different radicals of the same molecule ( $J_{\text{Gd-TEMPO}}/k_B = -6.45$  and  $+4.0$  K) [158]. Therefore, for a very anisotropic Dy, it is difficult to obtain more information due to the high mixing of the  $|J, m_J\rangle$  levels favored by the relatively low-symmetry ligand field in order to elucidate the nature of the exchange interactions in **38-Dy** [158].

The temperature dependence of  $\chi_m T$  for  $\text{Eu}^{3+}$  compounds is determined by the thermal population of the  ${}^7\text{F}_1$  level nearest to the non-magnetic ground level  ${}^7\text{F}_0$ . The excited  ${}^7\text{F}_1$  state, closely sited to the ground state, is already partly populated at room temperature. At 300 K,  $\chi_m T$  for  $\text{Eu}^{3+}$  complexes with diamagnetic organic ligands can vary in the range of 1.032–1.386 emu K/mol<sup>1</sup> depending on the ligand field parameters [159]. Therefore, for the complex **38-Eu**, the 300 K  $\chi_m T$  value of 1.778 emu K/mol is reasonable for the two uncoupled radicals and one  $\text{Eu}^{3+}$  ion, but a value lower than 1.93 emu K/mol was found for the bis-nitronyl nitroxide (NN) complex  $[\text{Eu}(\text{NN})_2(\text{NO}_3)_3]$  in a different coordination environment ( $\text{N}_{10}$  instead of  $\text{N}_4\text{O}_5$ ) [160]. As the temperature decreases, the  $\chi_m T$  decreases gradually, and, starting from 9 K, drops to 0.348 emu K/mol, which is somewhat higher than that for the  $[\text{Eu}(\text{NN})_2(\text{NO}_3)_3]$  compound (0.24 emu K/mol). No ac signal was observed in either sample in the measurable interval of frequencies (0.1–10,000 Hz).

#### 4.1.4. Rational Design of the Paramagnetic Tripods and Their Complexes

As mentioned above, in the presence of anionic ligands in the equatorial plane, it is better to use prolate Ln ions: Pm, Sm, Er, Tm, and Yb. While for more “magnetic” dysprosium and terbium, the presence of anionic ligands at the equator is strictly contraindicated. Therefore, it is necessary to change the molecular structure of the paramagnetic tripod so that there is no space for anionic ligands or solvent molecules in the Ln coordination sphere. An analysis of the molecular structure of the sandwich complexes with diamagnetic tripods has showed that the low-coordination compounds without anionic ligands are formed in the presence of steric hindrance in a position adjacent to donor tripod atoms, giving

propeller-like structures with ideal axially (see compounds **1**, **4**, **16**, **18**, **21**, and **31**). It should be noted that in most of the bis-tripodal complexes considered in this review, the ligands are symmetrical tripods, in contrast to the radical **35**, which consists of two six- and one five-membered hetero-cycles. Moreover, the paramagnetic tripod **35** comprises a bridgehead carbon atom. The other tripods described above are more spatial ligands compared to **35**. In complexes with the radical **35**, the average value for the side length of the triangular base is about 2.8 Å, while for the non-carbon bridgeheads, it is much larger: 2.9–3.1 for boron and 3.8–4.0 for nitrogen and metallic bridgehead. The larger dimensions to the tripods with hetero-bridgehead atoms “to more deeply set on the head” of the central Ln ion.

On the space filling image of the “burger” **38c** (Figure 7), it is clear that two pyridyl substituents of the different oxazolidine radicals **35** are in close proximity, and the shortest contact H . . . H between them is equal to 2.41 Å. In complex **40**, there are also sufficiently close distances between the pyridine rings and the methyl groups of the radical (2.613 and 3.007 Å, Figure 10a). Therefore, if an additional methyl group is located in the fourth position of the pyridyl rings (just near a donor nitrogen atom), then most likely, this will be enough for the paramagnetic tripods to turn relative to each other, resulting in the formation of a propeller-like structure in which there will be no place for additional molecules. In addition to increasing the steric load of the pyridyl substituents, it is necessary to make the paramagnetic tripod more symmetrical about the bridgehead carbon atom.

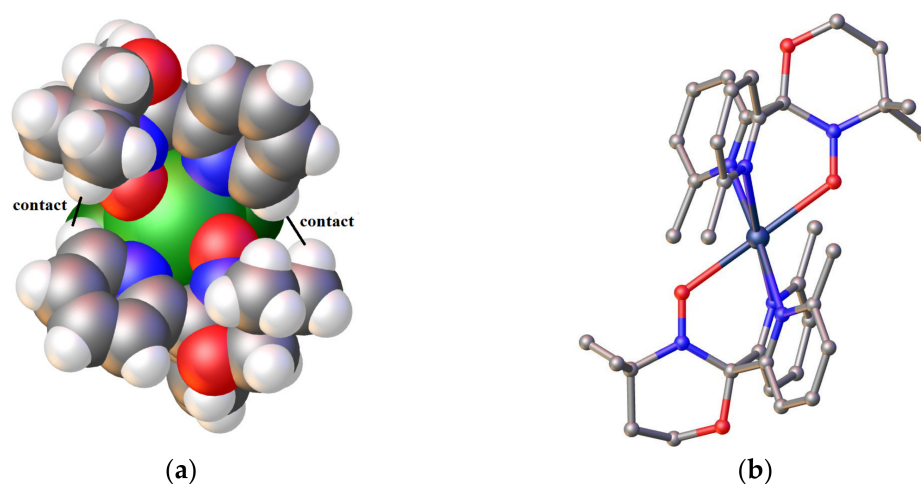
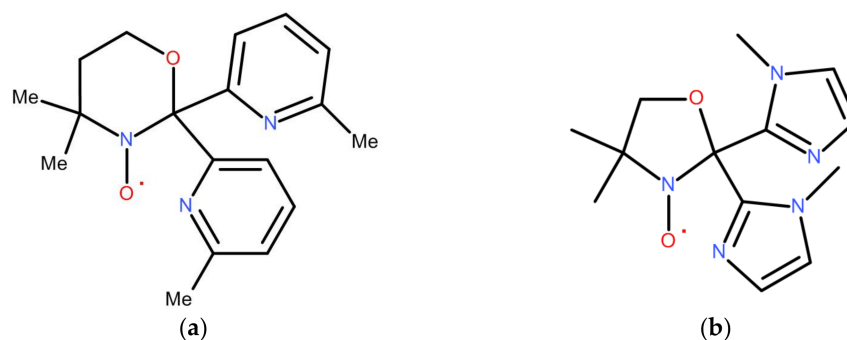


**Figure 10.** (a) The closest contacts in  $[\text{DyRad}_2\text{Cl}_2]^+$ ; (b) Bis-(oxazinane-radical) Ln complex cation.

Such a symmetrization can be performed by going from a five-membered oxazolidine ring to a six-membered oxazinane (**41**) (Scheme 2a and Figure 10b). The synthesis of such a tripodal radical becomes rather complicated due to commercially unavailable bis(6-methyl-2-pyridyl)methanone and 3-amino-3-methyl-butan-1-ol, the condensation of which yields its diamagnetic precursor.

The other way involves the choice of 1-imidazole as the functional group (instead of pyridine) for oxazolidine nitroxide (Scheme 2b). This is a slightly easier root because the starting aminoalcohol is cheap, but the corresponding bis-ketone must be prepared.

If the use of the hindered tripod **41** is intended to prevent the coordination of hetero-ligands in the equatorial plane, which is favorable for complexes with oblate Ln-ions, then its unhindered congener **42** is better to be used for heteroleptic complexes like **39** and **40** for the prolate lanthanide ion set. The latter can also be chosen for the heteroleptic complexes with the tripod **42**.



**Scheme 2.** More sterically demanding and symmetrical candidates as tripodal nitroxyl radicals: (a) 4,4-dimethyl-2,2-bis[2-(3-methylpyridyl)]oxazinane-N-oxyl (**41**); (b) 2,2-bis[2-(1-methylimidazol-2-yl)]oxazolidine-N-oxyl (**42**).

## 5. Conclusions

Despite numerous publications on the coordination chemistry and detailed crystallographic information of the lanthanide ions with tripodal ligands, their magnetic behavior has been poorly studied.

In contrast to the complexes of dysprosium and terbium, the coordination compounds of the prolate Pm, Sm, Er, Tm, and Yb are much less investigated. For the prolate ions, unhindered tripods with a shallow fit are more suitable, which makes it possible to ensure equatorial coordination of anionic hetero-ligands. Whereas, the sterically demanding tripods **41** are brilliantly suited for obtaining stable divalent Ln complexes [44,92], which is especially promising for the design of magneto-luminescent materials based on Eu(II) complexes, because their tricationic congener  $\text{Eu}^{3+}$  has a non-magnetic ground state.

This review of complexes with diamagnetic tripodal ligands was conducted with the hope that physicochemists will pay attention to this family of compounds and make more precise magneto-structural predictions based on CF parameters for the lanthanide ions in the respective ligand environments.

In magnetic terms, mono- and biradical Ln complexes are very interesting, but difficult for theoretical calculations. An important feature of the potential materials is their stability under normal conditions. Complexes with tripodal radicals possess this property. In addition, these paramagnetic tripods have a predictable type of coordination, which is extremely important in the rational design of compounds with desired properties.

The strong magnetic interaction between the radical center and the metal ion has a number of advantages for the design of advanced SIMs. For example, an additional unpaired electron of an organic radical may transform the resulting cationic complex into the Kramers system, while the initial free Ln-ion does not have this feature. In addition, the direct interaction of the unpaired 2p electron of the radical with the 4f shell removes the degeneracy of the energy levels, which can be useful for reducing QTM.

Without theoretical calculations, it is difficult to give precise prescriptions about the structure of a paramagnetic tripod for a particular lanthanide ion. However, we have tried to guess the general trend for the cyclic nitroxyl radicals functionalized by aromatic nitrogen-containing hetero-cycles: pyridine and imidazoline.

**Funding:** This research was funded by funded by Russian Science Foundation, Grant No. 23-23-00437, and partially supported by the Ministry of Science and Higher Education of the Russian Federation (crystal structure determination for the complexes with nitroxide radicals, 121031700313-8).

**Data Availability Statement:** Not applicable.

**Conflicts of Interest:** The author declares no conflict of interest.

## References

1. Szczepura, L.F.; Witham, L.M.; Takeuchi, K.J. Tris(2-Pyridyl) Tripod Ligands. *Coord. Chem. Rev.* **1998**, *174*, 5–32. [[CrossRef](#)]
2. Bellemin-Laponnaz, S.; Gade, L.H. A Modular Approach to C1 and C3 Chiral N-Tripodal Ligands for Asymmetric Catalysis. *Angew. Chem. Int. Ed.* **2002**, *41*, 3473–3475. [[CrossRef](#)]
3. Natrajan, L.; Pécaut, J.; Mazzanti, M.; LeBrun, C. Controlled Hydrolysis of Lanthanide Complexes of the N-Donor Tripod Tris(2-Pyridylmethyl)Amine versus Bisligand Complex Formation. *Inorg. Chem.* **2005**, *44*, 4756–4765. [[CrossRef](#)]
4. Chen, Y.-J.; Chen, H.-H. 1,1,1-Tris(Hydroxymethyl)Ethane as a New, Efficient, and Versatile Tripod Ligand for Copper-Catalyzed Cross-Coupling Reactions of Aryl Iodides with Amides, Thiols, and Phenols. *Org. Lett.* **2006**, *8*, 5609–5612. [[CrossRef](#)] [[PubMed](#)]
5. Eckert, M.; Brethon, A.; Li, Y.-X.; Sheldon, R.A.; Arends, I.W.C.E. Study of the Efficiency of Amino-Functionalized Ruthenium and Ruthenacycle Complexes as Racemization Catalysts in the Dynamic Kinetic Resolution of 1-Phenylethanol. *Adv. Synth. Catal.* **2007**, *349*, 2603–2609. [[CrossRef](#)]
6. Andrez, J.; Bozkoklu, G.; Nocton, G.; Pécaut, J.; Scopelliti, R.; Dubois, L.; Mazzanti, M. Lanthanide(II) Complexes Supported by N,O-Donor Tripodal Ligands: Synthesis, Structure, and Ligand-Dependent Redox Behavior. *Chem.-Eur. J.* **2015**, *21*, 15188–15200. [[CrossRef](#)]
7. Wietzke, R.; Mazzanti, M.; Latour, J.-M.; Pécaut, J.; Cordier, P.-Y.; Madić, C. Lanthanide(III) Complexes of Tripodal N-Donor Ligands: Structural Models for the Species Involved in Solvent Extraction of Actinides(III). *Inorg. Chem.* **1998**, *37*, 6690–6697. [[CrossRef](#)]
8. Kuswandi, B.; Nuriman, N.A.; Verboom, W.; Reinhoudt, D.N. Tripodal Receptors for Cation and Anion Sensors. *Sensors* **2006**, *6*, 978–1017. [[CrossRef](#)]
9. Dai, Z.; Canary, J.W. Tailoring Tripodal Ligands for Zinc Sensing. *New J. Chem.* **2007**, *31*, 1708–1718. [[CrossRef](#)]
10. Machado, K.; Mukhopadhyay, S.; Videira, R.A.; Mishra, J.; Mobin, S.M.; Mishra, G.S. Polymer Encapsulated Scorpionate Eu<sup>3+</sup> Complexes as Novel Hybrid Materials for High Performance Luminescence Applications. *RSC Adv.* **2015**, *5*, 35675–35682. [[CrossRef](#)]
11. Yu, T.; Zhao, Y.; Fan, D.; Hong, Z.; Su, W. Preparation, Photo- and Electro-Luminescent Properties of a Novel Complex of Tb(III) with a Tripod Ligand. *Spectrochim. Acta Part A Mol. Biomol. Spectrosc.* **2008**, *69*, 654–658. [[CrossRef](#)] [[PubMed](#)]
12. Long, J.; Lyubov, D.M.; Mahrova, T.V.; Lyssenko, K.A.; Korlyukov, A.A.; Fedorov, Y.V.; Chernikova, E.Y.; Guari, Y.; Larionova, J.; Trifonov, A.A. Heteroleptic Lanthanide Complexes Coordinated by Tripodal Tetradentate Ligand: Synthesis, Structure, and Magnetic and Photoluminescent Properties. *Cryst. Growth Des.* **2020**, *20*, 5184–5192. [[CrossRef](#)]
13. Zhu, L.; Tang, H.; Harima, Y.; Yamashita, K.; Hirayama, D.; Aso, Y.; Otsubo, T. Electrochemical Properties of Self-Assembled Monolayers of Tripod-Shaped Molecules and Their Applications to Organic Light-Emitting Diodes. *Chem. Commun.* **2001**, 1830–1831. [[CrossRef](#)]
14. Zheng, X.-L.; Liu, Y.; Pan, M.; Lü, X.-Q.; Zhang, J.-Y.; Zhao, C.-Y.; Tong, Y.-X.; Su, C.-Y. Bright Blue-Emitting Ce<sup>3+</sup> Complexes with Encapsulating Polybenzimidazole Tripodal Ligands as Potential Electroluminescent Devices. *Angew. Chem. Int. Ed.* **2007**, *46*, 7399–7403. [[CrossRef](#)] [[PubMed](#)]
15. Chen, K.-Y.; Ivashenko, O.; Carroll, G.T.; Robertus, J.; Kistemaker, J.C.M.; London, G.; Browne, W.R.; Rudolf, P.; Feringa, B.L. Control of Surface Wettability Using Tripodal Light-Activated Molecular Motors. *J. Am. Chem. Soc.* **2014**, *136*, 3219–3224. [[CrossRef](#)]
16. Kammerer, C.; Rapenne, G. Scorpionate Hydrotris(Indazolyl)Borate Ligands as Tripodal Platforms for Surface-Mounted Molecular Gears and Motors. *Eur. J. Inorg. Chem.* **2016**, *2016*, 2214–2226. [[CrossRef](#)]
17. Rabinovich, D. Synthetic Bioinorganic Chemistry: Scorpionates Turn 50. In *50 Years of Structure and Bonding—The Anniversary Volume*; Mingos, D.M.P., Ed.; Springer International Publishing: Cham, Switzerland, 2017; pp. 139–157, ISBN 978-3-319-35138-4.
18. Eliseeva, S.V.; Bünzli, J.-C.G. Lanthanide Luminescence for Functional Materials and Bio-Sciences. *Chem. Soc. Rev.* **2010**, *39*, 189–227. [[CrossRef](#)]
19. Klitsche, F.; Ramcke, J.; Migenda, J.; Hensel, A.; Vossmeier, T.; Weller, H.; Gross, S.; Maison, W. Synthesis of Tripodal Catecholates and Their Immobilization on Zinc Oxide Nanoparticles. *Beilstein J. Org. Chem.* **2015**, *11*, 678–686. [[CrossRef](#)]
20. Kurşunlu, A.N.; Özmen, M.; Güler, E. A Fluorescent Sensor-Based Tripodal-Bodipy for Cu (II) Ions: Bio-Imaging on Cells. *Turk. J. Chem.* **2021**, *45*, 2024–2033. [[CrossRef](#)]
21. Brechin, E.K. Using Tripodal Alcohols to Build High-Spin Molecules and Single-Molecule Magnets. *Chem. Commun.* **2005**, 5141–5153. [[CrossRef](#)]
22. Milios, C.J.; Manoli, M.; Rajaraman, G.; Mishra, A.; Budd, L.E.; White, F.; Parsons, S.; Wernsdorfer, W.; Christou, G.; Brechin, E.K. A Family of [Mn<sub>6</sub>] Complexes Featuring Tripodal Ligands. *Inorg. Chem.* **2006**, *45*, 6782–6793. [[CrossRef](#)]
23. Domingo, N.; Bellido, E.; Ruiz-Molina, D. Advances on Structuring, Integration and Magnetic Characterization of Molecular Nanomagnets on Surfaces and Devices. *Chem. Soc. Rev.* **2012**, *41*, 258–302. [[CrossRef](#)] [[PubMed](#)]
24. Long, J.; Lyubov, D.M.; Mahrova, T.V.; Cherkasov, A.V.; Fukin, G.K.; Guari, Y.; Larionova, J.; Trifonov, A.A. Synthesis, Structure and Magnetic Properties of Tris(Pyrazolyl)Methane Lanthanide Complexes: Effect of the Anion on the Slow Relaxation of Magnetization. *Dalton Trans.* **2018**, *47*, 5153–5156. [[CrossRef](#)] [[PubMed](#)]
25. Ito, A.; Nakano, Y.; Urabe, M.; Tanaka, K.; Shiro, M. Structural and Magnetic Studies of Copper(II) and Zinc(II) Coordination Complexes Containing Nitroxide Radicals as Chelating Ligands. *Eur. J. Inorg. Chem.* **2006**, *2006*, 3359–3368. [[CrossRef](#)]

26. Gass, I.A.; Gartshore, C.J.; Lupton, D.W.; Moubaraki, B.; Nafady, A.; Bond, A.M.; Boas, J.F.; Cashion, J.D.; Milsmann, C.; Wieghardt, K.; et al. Anion Dependent Redox Changes in Iron Bis-Terdentate Nitroxide {NNO} Chelates. *Inorg. Chem.* **2011**, *50*, 3052–3064. [[CrossRef](#)] [[PubMed](#)]
27. Gass, I.A.; Tewary, S.; Nafady, A.; Chilton, N.F.; Gartshore, C.J.; Asadi, M.; Lupton, D.W.; Moubaraki, B.; Bond, A.M.; Boas, J.F.; et al. Observation of Ferromagnetic Exchange, Spin Crossover, Reductively Induced Oxidation, and Field-Induced Slow Magnetic Relaxation in Monomeric Cobalt Nitroxides. *Inorg. Chem.* **2013**, *52*, 7557–7572. [[CrossRef](#)]
28. Gass, I.A.; Tewary, S.; Rajaraman, G.; Asadi, M.; Lupton, D.W.; Moubaraki, B.; Chastanet, G.; Létard, J.-F.; Murray, K.S. Solvate-Dependent Spin Crossover and Exchange in Cobalt(II) Oxazolidine Nitroxide Chelates. *Inorg. Chem.* **2014**, *53*, 5055–5066. [[CrossRef](#)]
29. Gass, I.A.; Asadi, M.; Lupton, D.W.; Moubaraki, B.; Bond, A.M.; Guo, S.-X.; Murray, K.S. Manganese(II) Oxazolidine Nitroxide Chelates: Structure, Magnetism, and Redox Properties. *Aust. J. Chem.* **2014**, *67*, 1618–1624. [[CrossRef](#)]
30. Pedersen, A.H.; Geoghegan, B.L.; Nichol, G.S.; Lupton, D.W.; Murray, K.S.; Martínez-Lillo, J.; Gass, I.A.; Brechin, E.K. Hexahalorhenate(IV) Salts of Metal Oxazolidine Nitroxides. *Dalton Trans.* **2017**, *46*, 5250–5259. [[CrossRef](#)]
31. Gass, I.A.; Lu, J.; Asadi, M.; Lupton, D.W.; Forsyth, C.M.; Geoghegan, B.L.; Moubaraki, B.; Cashion, J.D.; Martin, L.L.; Bond, A.M.; et al. Use of the TCNQF<sub>4</sub><sup>2-</sup> Dianion in the Spontaneous Redox Formation of [Fe<sup>III</sup>(L<sup>-</sup>)<sub>2</sub>][TCNQF<sub>4</sub><sup>-</sup>]. *Chempluschem* **2018**, *83*, 658–668. [[CrossRef](#)]
32. Gass, I.A.; Lu, J.; Ojha, R.; Asadi, M.; Lupton, D.W.; Geoghegan, B.L.; Moubaraki, B.; Martin, L.L.; Bond, A.M.; Murray, K.S. [Fe<sup>II</sup>(L<sup>•</sup>)<sub>2</sub>][TCNQF<sub>4</sub><sup>•-</sup>]<sub>2</sub>: A Redox-Active Double Radical Salt. *Aust. J. Chem.* **2019**, *72*, 769–777. [[CrossRef](#)]
33. Trofimenko, S. Boron-Pyrazole Chemistry. *J. Am. Chem. Soc.* **1966**, *88*, 1842–1844. [[CrossRef](#)]
34. Oliver, J.D.; Mullica, D.F.; Hutchinson, B.B.; Milligan, W.O. Iron-Nitrogen Bond Lengths in Low-Spin and High-Spin Iron(II) Complexes with Poly(Pyrazolyl)Borate Ligands. *Inorg. Chem.* **1980**, *19*, 165–169. [[CrossRef](#)]
35. Trofimenko, S. Recent Advances in Poly(Pyrazolyl)Borate (Scorpionate) Chemistry. *Chem. Rev.* **1993**, *93*, 943–980. [[CrossRef](#)]
36. Wu, L.P.; Yamagiwa, Y.; Ino, I.; Sugimoto, K.; Kuroda-Sowa, T.; Kamikawa, T.; Munakata, M. Unique Tetranuclear Copper(II) Cluster and Monomeric Iron(II), (III) Complexes with a Tris(Imidazolyl) Chelating Ligand. *Polyhedron* **1999**, *18*, 2047–2053. [[CrossRef](#)]
37. Pettinari, C. (Ed.) *Scorpionates II: Chelating Borate Ligands-Dedicated to Swiatoslaw Trofimenko*; Imperial College Press and Distributed by World Scientific: London, UK, 2008; ISBN 978-1-86094-876-3.
38. Dougherty, W.G.; Kassel, W.S. Synthesis of a Series of First-Row Tris-Imidazolylphosphine Sandwich Complexes and Their Potential for Formation of Polymetallic Species. *Inorganica Chim. Acta* **2010**, *364*, 120–124. [[CrossRef](#)]
39. Saouma, C.T.; Peters, J.C. ME and ME Complexes of Iron and Cobalt That Emphasize Three-Fold Symmetry (E = O, N, NR). *Coord. Chem. Rev.* **2011**, *255*, 920–937. [[CrossRef](#)]
40. Lavrenova, L.G.; Strekalova, A.D.; Smolentsev, A.I.; Naumov, D.Y.; Bogomyakov, A.S.; Sheludyakova, L.A.; Vasilevskii, S.F. Mono- and Heteroligand Iron(II) Complexes with Tris(3,5-Dimethylpyrazol-1-Yl)Methane. *Russ. J. Coord. Chem.* **2016**, *42*, 711–718. [[CrossRef](#)]
41. Feng, M.; Tong, M.-L. Single Ion Magnets from 3d to 5f: Developments and Strategies. *Chem.-Eur. J.* **2018**, *24*, 7574–7594. [[CrossRef](#)]
42. Landart-Gereka, A.; Quesada-Moreno, M.M.; Palacios, M.A.; Díaz-Ortega, I.F.; Nojiri, H.; Ozerov, M.; Krzystek, J.; Colacio, E. Pushing up the Easy-Axis Magnetic Anisotropy and Relaxation Times in Trigonal Prismatic Co<sup>II</sup> Mononuclear SMMs by Molecular Structure Design. *Chem. Commun.* **2023**, *59*, 952–955. [[CrossRef](#)]
43. Apostolidis, C.; Carvalho, A.; Domingos, A.; Kanellakopulos, B.; Maier, R.; Marques, N.; de Matos, A.P.; Rebizant, J. Chloro-Lanthanide, and Plutonium Complexes Containing the Hydrotris(3,5-Dimethylpyrazol-1-Yl)Borate Ligand: The Crystal and Molecular Structures of [PrCl(μ-Cl)Tp<sup>Me2</sup>(3,5-Me<sub>2</sub>pzH)]<sub>2</sub> and YbCl<sub>2</sub>Tp<sup>Me2</sup>(THF). *Polyhedron* **1998**, *18*, 263–272. [[CrossRef](#)]
44. Hillier, A.C.; Zhang, X.W.; Maunder, G.H.; Liu, S.Y.; Eberspacher, T.A.; Metz, M.V.; McDonald, R.; Domingos, A.; Marques, N.; Day, V.W.; et al. Synthesis and Structural Comparison of a Series of Divalent Ln(Tp<sup>R,R</sup>)<sub>2</sub> (Ln = Sm, Eu, Yb) and Trivalent Sm(Tp<sup>Me2</sup>)<sub>2</sub>X (X = F, Cl, I, BPh<sub>4</sub>) Complexes. *Inorg. Chem.* **2001**, *40*, 5106–5116. [[CrossRef](#)] [[PubMed](#)]
45. Sella, A.; Brown, S.E.; Steed, J.W.; Tocher, D.A. Synthesis and Solid-State Structures of Pyrazolylmethane Complexes of the Rare Earths. *Inorg. Chem.* **2007**, *46*, 1856–1864. [[CrossRef](#)] [[PubMed](#)]
46. Liu, S.-Y.; Maunder, G.H.; Sella, A.; Stevenson, M.; Tocher, D.A. Synthesis and Molecular Structures of Hydrotris(Dimethylpyrazolyl)-Borate Complexes of the Lanthanides. *Inorg. Chem.* **1996**, *35*, 76–81. [[CrossRef](#)] [[PubMed](#)]
47. Werner, E.J.; Biro, S.M. Supramolecular Ligands for the Extraction of Lanthanide and Actinide Ions. *Org. Chem. Front.* **2019**, *6*, 2067–2094. [[CrossRef](#)]
48. Barraza, R.; Sertage, A.G.; Kajjam, A.B.; Ward, C.L.; Lutter, J.C.; Schlegel, H.B.; Allen, M.J. Properties of Amine-Containing Ligands That Are Necessary for Visible-Light-Promoted Catalysis with Divalent Europium. *Inorg. Chem.* **2022**, *61*, 19649–19657. [[CrossRef](#)]
49. Frost, J.M.; Harriman, K.L.M.; Murugesu, M. The Rise of 3-d Single-Ion Magnets in Molecular Magnetism: Towards Materials from Molecules? *Chem. Sci.* **2016**, *7*, 2470–2491. [[CrossRef](#)]
50. Zhu, Z.; Guo, M.; Li, X.-L.; Tang, J. Molecular Magnetism of Lanthanide: Advances and Perspectives. *Coord. Chem. Rev.* **2019**, *378*, 350–364. [[CrossRef](#)]

51. Zabala-Lekuona, A.; Seco, J.M.; Colacio, E. Single-Molecule Magnets: From Mn<sub>12</sub>-Ac to Dysprosium Metallocenes, a Travel in Time. *Coord. Chem. Rev.* **2021**, *441*, 213984. [[CrossRef](#)]
52. Gatteschi, D.; Sessoli, R. Quantum Tunneling of Magnetization and Related Phenomena in Molecular Materials. *Angew. Chem. Int. Ed.* **2003**, *42*, 268–297. [[CrossRef](#)]
53. Goodwin, C.A.P.; Ortu, F.; Reta, D. Strangely Attractive: Collaboration and Feedback in the Field of Molecular Magnetism. *Int. J. Quantum Chem.* **2020**, *120*, e26248. [[CrossRef](#)]
54. Tang, J.; Zhang, P. *Lanthanide Single Molecule Magnets*; Springer: Berlin/Heidelberg, Germany, 2015; ISBN 978-3-662-46998-9.
55. Sorace, L.; Gatteschi, D. Electronic Structure and Magnetic Properties of Lanthanide Molecular Complexes. In *Lanthanides and Actinides in Molecular Magnetism*; Wiley-VCH Verlag GmbH & Co. KGaA: Weinheim, Germany, 2015; pp. 1–26.
56. Goodwin, C.A.P.; Ortu, F.; Reta, D.; Chilton, N.F.; Mills, D.P. Molecular Magnetic Hysteresis at 60 Kelvin in Dysprosocenium. *Nature* **2017**, *548*, 439–442. [[CrossRef](#)]
57. Guo, F.-S.; Day, B.M.; Chen, Y.-C.; Tong, M.-L.; Mansikkamäki, A.; Layfield, R.A. A Dysprosium Metallocene Single-Molecule Magnet Functioning at the Axial Limit. *Angew. Chem. Int. Ed.* **2017**, *56*, 11445–11449. [[CrossRef](#)]
58. Guo, F.-S.; Day, B.M.; Chen, Y.-C.; Tong, M.-L.; Mansikkamäki, A.; Layfield, R.A. Magnetic Hysteresis up to 80 Kelvin in a Dysprosium Metallocene Single-Molecule Magnet. *Science* **2018**, *362*, 1400–1403. [[CrossRef](#)]
59. Vincent, A.H.; Whyatt, Y.L.; Chilton, N.F.; Long, J.R. Strong Axiality in a Dysprosium(III) Bis(Borolide) Complex Leads to Magnetic Blocking at 65 K. *J. Am. Chem. Soc.* **2023**, *145*, 1572–1579. [[CrossRef](#)]
60. Rinehart, J.D.; Long, J.R. Exploiting Single-Ion Anisotropy in the Design of f-Element Single-Molecule Magnets. *Chem. Sci.* **2011**, *2*, 2078–2085. [[CrossRef](#)]
61. Chilton, N.F. Design Criteria for High-Temperature Single-Molecule Magnets. *Inorg. Chem.* **2015**, *54*, 2097–2099. [[CrossRef](#)]
62. Harriman, K.L.M.; Errulat, D.; Murugesu, M. Magnetic Axiality: Design Principles from Molecules to Materials. *Trends Chem.* **2019**, *1*, 425–439. [[CrossRef](#)]
63. Guo, F.-S.; Bar, A.K.; Layfield, R.A. Main Group Chemistry at the Interface with Molecular Magnetism. *Chem. Rev.* **2019**, *119*, 8479–8505. [[CrossRef](#)]
64. Chiesa, A.; Cugini, F.; Hussain, R.; Macaluso, E.; Allodi, G.; Garlatti, E.; Giansiracusa, M.; Goodwin, C.A.P.; Ortu, F.; Reta, D.; et al. Understanding Magnetic Relaxation in Single-Ion Magnets with High Blocking Temperature. *Phys. Rev. B* **2020**, *101*, 174402. [[CrossRef](#)]
65. Woodruff, D.N.; Winpenny, R.E.P.; Layfield, R.A. Lanthanide Single-Molecule Magnets. *Chem. Rev.* **2013**, *113*, 5110–5148. [[CrossRef](#)] [[PubMed](#)]
66. Jiang, S.-D.; Wang, B.-W.; Gao, S. Advances in Lanthanide Single-Ion Magnets. In *Molecular Nanomagnets and Related Phenomena*; Gao, S., Ed.; Springer: Berlin/Heidelberg, Germany, 2015; pp. 111–141, ISBN 978-3-662-45723-8.
67. Gupta, S.K.; Murugavel, R. Enriching Lanthanide Single-Ion Magnetism through Symmetry and Axiality. *Chem. Commun.* **2018**, *54*, 3685–3696. [[CrossRef](#)] [[PubMed](#)]
68. Vogel, R.; Müntener, T.; Häussinger, D. Intrinsic Anisotropy Parameters of a Series of Lanthanoid Complexes Deliver New Insights into the Structure-Magnetism Relationship. *Chem* **2021**, *7*, 3144–3156. [[CrossRef](#)]
69. Jiang, S.-D.; Qin, S.-X. Prediction of the Quantized Axis of Rare-Earth Ions: The Electrostatic Model with Displaced Point Charges. *Inorg. Chem. Front.* **2015**, *2*, 613–619. [[CrossRef](#)]
70. Liu, J.-L.; Chen, Y.-C.; Tong, M.-L. Symmetry Strategies for High Performance Lanthanide-Based Single-Molecule Magnets. *Chem. Rev.* **2018**, *47*, 2431–2453. [[CrossRef](#)]
71. Chen, Y.-C.; Tong, M.-L. Single-Molecule Magnets beyond a Single Lanthanide Ion: The Art of Coupling. *Chem. Sci.* **2022**, *13*, 8716–8726. [[CrossRef](#)]
72. Gao, S. (Ed.) *Molecular Nanomagnets and Related Phenomena—Structure and Bonding*; Springer: Berlin/Heidelberg, Germany, 2015; ISBN 978-3-662-45722-1.
73. Kahn, O. *Molecular Magnetism*; VCH: New York, NY, USA, 1993; ISBN 978-1-56081-566-2.
74. Boča, R. *Theoretical Foundations of Molecular Magnetism*; In the Series, Current Methods in Inorganic Chemistry, Vol. 1; Elsevier: Amsterdam, The Netherlands, 1999; Volume 1, p. 874, ISBN 0-444-50229-7.
75. Chen, Y.-C.; Liu, J.-L.; Wernsdorfer, W.; Liu, D.; Chibotaru, L.F.; Chen, X.-M.; Tong, M.-L. Hyperfine-Interaction-Driven Suppression of Quantum Tunneling at Zero Field in a Holmium(III) Single-Ion Magnet. *Angew. Chem. Int. Ed.* **2017**, *56*, 4996–5000. [[CrossRef](#)]
76. Skomski, R.; Sellmyer, D.J. Anisotropy of Rare-Earth Magnets. *J. Rare Earths* **2009**, *27*, 675–679. [[CrossRef](#)]
77. Zhu, Z.; Tang, J. Lanthanide Single-Molecule Magnets with High Anisotropy Barrier: Where to from Here? *Natl. Sci. Rev.* **2022**, *9*, nwac194. [[CrossRef](#)]
78. Wang, J.; Sun, C.; Zheng, Q.; Wang, D.; Chen, Y.; Ju, J.; Sun, T.; Cui, Y.; Ding, Y.; Tang, Y. Lanthanide Single-molecule Magnets: Synthetic Strategy, Structures, Properties and Recent Advances. *Chem.—Asian J.* **2023**, *18*, e202201297. [[CrossRef](#)]
79. Trofimenko, S. *The Coordination Chemistry of Polypyrazolylborate Ligand*; Imperial College Press: London, UK, 1999; ISBN 978-1-86094-172-6.
80. Cheng, J.; Takats, J.; Ferguson, M.J.; McDonald, R. Heteroleptic Tm(II) Complexes: One More Success for Trofimenko's Scorpi-onates. *J. Am. Chem. Soc.* **2008**, *130*, 1544–1545. [[CrossRef](#)]

81. Dei, A.; Gatteschi, D.; Pécaut, J.; Poussereau, S.; Sorace, L.; Vostrikova, K. Crystal Field and Exchange Effects in Rare Earth Semiquinone Complexes. *Comptes Rendus l'Academie Sci.-Ser. IIC-Chem.* **2001**, *4*, 135–141. [[CrossRef](#)]
82. Zhang, P.; Perfetti, M.; Kern, M.; Hallmen, P.P.; Ungur, L.; Lenz, S.; Ringenberg, M.R.; Frey, W.; Stoll, H.; Rauhut, G.; et al. Exchange Coupling and Single Molecule Magnetism in Redox-Active Tetraoxolene-Bridged Dilanthanide Complexes. *Chem. Sci.* **2018**, *9*, 1221–1230. [[CrossRef](#)]
83. Xu, G.-F.; Gamez, P.; Tang, J.; Clérac, R.; Guo, Y.-N.; Guo, Y.  $M^{III}Dy^{III}_3$  ( $M = Fe^{III}, Co^{III}$ ) Complexes: Three-Blade Propellers Exhibiting Slow Relaxation of Magnetization. *Inorg. Chem.* **2012**, *51*, 5693–5698. [[CrossRef](#)]
84. Xu, G.-F.; Wang, Q.-L.; Gamez, P.; Ma, Y.; Clérac, R.; Tang, J.; Yan, S.-P.; Cheng, P.; Liao, D.-Z. A Promising New Route towards Single-Molecule Magnets Based on the Oxalate Ligand. *Chem. Commun.* **2010**, *46*, 1506–1508. [[CrossRef](#)]
85. Mikhalyova, E.A.; Zeller, M.; Jasinski, J.P.; Butcher, R.J.; Carrella, L.M.; Sedykh, A.E.; Gavrilenko, K.S.; Smola, S.S.; Frasso, M.; Cazorla, S.C.; et al. Combination of Single-Molecule Magnet Behaviour and Luminescence Properties in a New Series of Lanthanide Complexes with Tris(Pyrazolyl)Borate and Oligo( $\beta$ -Diketonate) Ligands. *Dalton Trans.* **2020**, *49*, 7774–7789. [[CrossRef](#)]
86. Kandel, A.V.; Mikhalyova, E.A.; Zeller, M.; Addison, A.W.; Pavlishchuk, V.V. Influence of the Structure of 3-Arylacetylacetonate Ligands on the Luminescence Properties of  $Eu^{3+}$  and  $Tb^{3+}$  Complexes. *Theor. Exp. Chem.* **2017**, *53*, 180–186. [[CrossRef](#)]
87. Depperman, E.C.; Bodnar, S.H.; Vostrikova, K.E.; Shultz, D.A.; Kirk, M.L. Spin Robustness of a New Hybrid Inorganic–Organic High-Spin Molecule. *J. Am. Chem. Soc.* **2001**, *123*, 3133–3134. [[CrossRef](#)]
88. Wang, S.; Zuo, J.-L.; Zhou, H.-C.; Choi, H.J.; Ke, Y.; Long, J.R.; You, X.-Z.  $[(Tp)_8(H_2O)_6Cu^{II}_6Fe^{III}_8(CN)_{24}]^{4+}$ : A Cyanide-Bridged Face-Centered-Cubic Cluster with Single-Molecule-Magnet Behavior. *Angew. Chem. Int. Ed.* **2004**, *43*, 5940–5943. [[CrossRef](#)]
89. Wang, S.; Zuo, J.-L.; Gao, S.; Song, Y.; Zhou, H.-C.; Zhang, Y.-Z.; You, X.-Z. The Observation of Superparamagnetic Behavior in Molecular Nanowires. *J. Am. Chem. Soc.* **2004**, *126*, 8900–8901. [[CrossRef](#)]
90. Alexandropoulos, D.I.; Vignesh, K.R.; Xie, H.; Dunbar, K.R. Switching on Single-Molecule Magnet Properties of Homoleptic Sandwich Tris(Pyrazolyl)Borate Dysprosium(III) Cations via Intermolecular Dipolar Coupling. *Dalton Trans.* **2019**, *48*, 10610–10618. [[CrossRef](#)] [[PubMed](#)]
91. Kühling, M.; Wickleder, C.; Ferguson, M.J.; Hrib, C.G.; McDonald, R.; Suta, M.; Hilfert, L.; Takats, J.; Edelmann, F.T. Investigation of the “Bent Sandwich-like” Divalent Lanthanide Hydro-Tris(Pyrazolyl)Borates  $Ln(Tp^{iPr}_2)_2$  ( $Ln = Sm, Eu, Tm, Yb$ ). *New J. Chem.* **2015**, *39*, 7617–7625. [[CrossRef](#)]
92. Qi, H.; Zhao, Z.; Zhan, G.; Sun, B.; Yan, W.; Wang, C.; Wang, L.; Liu, Z.; Bian, Z.; Huang, C. Air Stable and Efficient Rare Earth Eu(II) Hydro-Tris(Pyrazolyl)Borate Complexes with Tunable Emission Colors. *Inorg. Chem. Front.* **2020**, *7*, 4593–4599. [[CrossRef](#)]
93. Takats, J.; Zhang, X.W.; Day, V.W.; Eberspacher, T.A. Synthesis and Structure of Bis[Hydrotris(3,5-Dimethylpyrazolyl)Borato]-Samarium(II),  $Sm[HB(3,5-Me_2pz)_3]_2$ , and the Product of Its Reaction with Azobenzene. *Organometallics* **1993**, *12*, 4286–4288. [[CrossRef](#)]
94. Maunder, G.H.; Sella, A.; Tocher, D.A. Synthesis and Molecular Structures of a Redox-Related Pair of Lanthanide Complexes. *J. Chem. Soc. Chem. Commun.* **1994**, 885. [[CrossRef](#)]
95. Momin, A.; Carter, L.; Yang, Y.; McDonald, R.; Essafi (née Labouille), S.; Nief, F.; Del Rosal, I.; Sella, A.; Maron, L.; Takats, J. To Bend or Not To Bend: Experimental and Computational Studies of Structural Preference in  $Ln(Tp^{iPr}_2)_2$  ( $Ln = Sm, Tm$ ). *Inorg. Chem.* **2014**, *53*, 12066–12075. [[CrossRef](#)]
96. Saliu, K.O.; Takats, J.; Ferguson, M.J. Bis[Tris(3-tert-butyl-5-Methylpyrazol-1-Yl)Hydridoborato]Ytterbium(II) Toluene Solvate. *Acta Crystallogr. Sect. E Struct. Rep. Online* **2009**, *65*, m643–m644. [[CrossRef](#)]
97. Suta, M.; Kühling, M.; Liebing, P.; Edelmann, F.T.; Wickleder, C. Photoluminescence Properties of the “Bent Sandwich-like” Compounds  $[Eu(Tp^{iPr}_2)_2]$  and  $[Yb(Tp^{iPr}_2)_2]$ —Intermediates between Nitride-Based Phosphors and Metallocenes. *J. Lumin.* **2017**, *187*, 62–68. [[CrossRef](#)]
98. Arikawa, Y.; Inada, K.; Onishi, M. Side-on Coordination Mode of a Pyrazolyl Group in the Structure of a Divalent  $[Sm\{B(3-Mepz)_4\}_2]$  Complex (3-Mepz Is 3-Methylpyrazol-1-Yl). *Acta Crystallogr. Sect. C Struct. Chem.* **2016**, *72*, 838–841. [[CrossRef](#)]
99. Li, Z.-H.; Zhai, Y.-Q.; Chen, W.-P.; Ding, Y.-S.; Zheng, Y.-Z. Air-Stable Hexagonal Bipyramidal Dysprosium(III) Single-Ion Magnets with Nearly Perfect  $D_{6h}$  Local Symmetry. *Chem.-Eur. J.* **2019**, *25*, 16219–16224. [[CrossRef](#)]
100. Canaj, A.B.; Dey, S.; Martí, E.R.; Wilson, C.; Rajaraman, G.; Murrie, M. Insight into  $D_{6h}$  Symmetry: Targeting Strong Axiality in Stable Dysprosium(III) Hexagonal Bipyramidal Single-Ion Magnets. *Angew. Chem. Int. Ed.* **2019**, *58*, 14146–14151. [[CrossRef](#)]
101. Li, Q.-W.; Wan, R.-C.; Chen, Y.-C.; Liu, J.-L.; Wang, L.-F.; Jia, J.-H.; Chilton, N.F.; Tong, M.-L. Unprecedented Hexagonal Bipyramidal Single-Ion Magnets Based on Metallacrowns. *Chem. Commun.* **2016**, *52*, 13365–13368. [[CrossRef](#)]
102. Gil, Y.; Castro-Alvarez, A.; Fuentealba, P.; Spodine, E.; Aravena, D. Lanthanide SMMs Based on Belt Macrocycles: Recent Advances and General Trends. *Chem.-Eur. J.* **2022**, *28*, e202200336. [[CrossRef](#)]
103. Meyer, G. All the Lanthanides Do It and Even Uranium Does Oxidation State +2. *Angew. Chem. Int. Ed.* **2014**, *53*, 3550–3551. [[CrossRef](#)]
104. Llunell, M.; Casanova, D.; Cirera, J.; Alemany, P.; Alvarez, S. *SHAPE, Version 2.1, Program for the Stereochemical Analysis of Molecular Fragments by Means of Continuous Shape Measures and Associated Tools*; Universitat de Barcelona: Barcelona, Spain, 2013; Volume 2103.
105. Li, T.; Zhang, G.; Guo, J.; Wang, S.; Leng, X.; Chen, Y. Tris(Pyrazolyl)Methanide Complexes of Trivalent Rare-Earth Metals. *Organometallics* **2016**, *35*, 1565–1572. [[CrossRef](#)]

106. Keene, F.R.; Snow, M.R.; Stephenson, P.J.; Tiekink, E.R.T. Ruthenium(II) Complexes of the C<sub>3v</sub> Ligands Tris(2-Pyridyl)Amine, Tris(2-Pyridyl)Methane, and Tris(2-Pyridyl)Phosphine. 1. Synthesis and x-Ray Structural Studies of the Bis(Ligand) Complexes. *Inorg. Chem.* **1988**, *27*, 2040–2045. [[CrossRef](#)]
107. García, F.; Hopkins, A.D.; Humphrey, S.M.; McPartlin, M.; Rogers, M.C.; Wright, D.S. The First Example of a Si-Bridged Tris(Pyridyl) Ligand; Synthesis and Structure of [MeSi(2-C<sub>5</sub>H<sub>4</sub>N)<sub>3</sub>LiX] (X = 0.2Br, 0.8Cl). *Dalton Trans.* **2004**, 361–362. [[CrossRef](#)]
108. Mann, F.G.; Watson, J. Conditions of Salt Formation in Polyamines and Kindred Compounds. Salt Formation in the Tertiary 2-Pyridylamines, Phosphines and Arsines. *J. Org. Chem.* **1948**, *13*, 502–531. [[CrossRef](#)]
109. García, F.; Hopkins, A.D.; Kowenicki, R.A.; McPartlin, M.; Rogers, M.C.; Silvia, J.S.; Wright, D.S. Syntheses and Structure of Heterometallic Complexes Containing Tripodal Group 13 Ligands [RE(2-Py)<sub>3</sub>]<sup>−</sup> (E = Al, In). *Organometallics* **2006**, *25*, 2561–2568. [[CrossRef](#)]
110. Beswick, M.A.; Belle, C.J.; Davies, M.K.; Halcrow, M.A.; Raithby, P.R.; Steiner, A.; Wright, D.S. One-Pot Synthesis of a Novel Tridentate Tin(IV) Ligand; Syntheses and Structures of [BunSn(NC<sub>5</sub>H<sub>4</sub>-C,N)<sub>3</sub>MBr](M = Li, Cu). *Chem. Commun.* **1996**, 2619. [[CrossRef](#)]
111. Zeckert, K.; Zahn, S.; Kirchner, B. Tin–Lanthanoid Donor–Acceptor Bonds. *Chem. Commun.* **2010**, *46*, 2638. [[CrossRef](#)] [[PubMed](#)]
112. Beswick, M.A.; Davies, M.K.; Raithby, P.R.; Steiner, A.; Wright, D.S. Synthesis and Structure of [Pb(2-Py)<sub>3</sub>Li·THF], Containing a Low-Valent Group 14 Tris(Pyridyl) Ligand (2-Py = 2-Pyridyl). *Organometallics* **1997**, *16*, 1109–1110. [[CrossRef](#)]
113. Goura, J.; McQuade, J.; Shimoyama, D.; Lalancette, R.A.; Sheridan, J.B.; Jäkle, F. Electrophilic and Nucleophilic Displacement Reactions at the Bridgehead Borons of Tris(Pyridyl)Borate Scorpionate Complexes. *Chem. Commun.* **2022**, *58*, 977–980. [[CrossRef](#)] [[PubMed](#)]
114. Reichart, F.; Kischel, M.; Zeckert, K. Lanthanide(II) Complexes of a Dual Functional Tris(2-Pyridyl)Stannate Derivative. *Chem.-Eur. J.* **2009**, *15*, 10018–10020. [[CrossRef](#)] [[PubMed](#)]
115. Zeckert, K. Syntheses and Structures of Lanthanoid(II) Complexes Featuring Sn–M (M = Al, Ga, In) Bonds. *Dalton Trans.* **2012**, *41*, 14101–14106. [[CrossRef](#)]
116. Zeckert, K. Pyridyl Compounds of Heavier Group 13 and 14 Elements as Ligands for Lanthanide Metals. *Organometallics* **2013**, *32*, 1387–1393. [[CrossRef](#)]
117. Zeckert, K.; Griebel, J.; Kirmse, R.; Weiß, M.; Denecke, R. Versatile Reactivity of a Lithium Tris(Aryl)Plumbate(II) Towards Organolanthanoid Compounds: Stable Lead–Lanthanoid–Metal Bonds or Redox Processes. *Chem.-Eur. J.* **2013**, *19*, 7718–7722. [[CrossRef](#)]
118. Hellmann, K.W.; Gade, L.H.; Gevert, O.; Steinert, P.; Lauher, J.W. Tripodal Triamidostannates and -Plumbates. *Inorg. Chem.* **1995**, *34*, 4069–4078. [[CrossRef](#)]
119. García-Rodríguez, R.; Simmonds, H.R.; Wright, D.S. Formation of a Heterometallic AlIII/SmIII Complex Involving a Novel [EtAl(2-Py)<sub>2</sub>O]<sup>2−</sup> Ligand (2-Py = 2-Pyridyl). *Organometallics* **2014**, *33*, 7113–7117. [[CrossRef](#)]
120. García-Rodríguez, R.; Kopf, S.; Wright, D.S. Modifying the Donor Properties of Tris(Pyridyl)Aluminates in Lanthanide(Ii) Sandwich Compounds. *Dalton Trans.* **2018**, *47*, 2232–2239. [[CrossRef](#)]
121. Hajjashrafi, T.; Nemati Kharat, A.; Love, J.A.; Patrick, B.O. Synthesis, Characterization and Crystal Structure of Three New Lanthanide (III) Complexes with the [(6-Methyl-2-Pyridyl)Methyl]Bis(2-Pyridylmethyl)Amine (MeTPA) Ligand; New Precursors for Lanthanide (III) Oxide Nano-Particles. *Polyhedron* **2013**, *60*, 30–38. [[CrossRef](#)]
122. Hay, M.A.; Gable, R.W.; Boskovic, C. Modulating the Electronic Properties of Divalent Lanthanoid Complexes with Subtle Ligand Tuning. *Dalton Trans.* **2023**, *52*, 3315–3324. [[CrossRef](#)]
123. Zhang, C.; Cheng, Z.; Tan, P.; Lv, W.; Cui, H.; Chen, L.; Cai, X.; Zhao, Y.; Yuan, A. Tuning the Ligand Field in Seven-Coordinate Dy(III) Complexes to Perturb Single-Ion Magnet Behavior. *New J. Chem.* **2021**, *45*, 8591–8596. [[CrossRef](#)]
124. Demir, S.; Jeon, I.-R.; Long, J.R.; Harris, T.D. Radical Ligand-Containing Single-Molecule Magnets. *Coord. Chem. Rev.* **2015**, *289–290*, 149–176. [[CrossRef](#)]
125. Ishikawa, N.; Sugita, M.; Tanaka, N.; Ishikawa, T.; Koshihara, S.; Kaizu, Y. Upward Temperature Shift of the Intrinsic Phase Lag of the Magnetization of Bis(Phthalocyaninato)Terbium by Ligand Oxidation Creating an S = 1/2 Spin. *Inorg. Chem.* **2004**, *43*, 5498–5500. [[CrossRef](#)]
126. Pederson, R.; Wysocki, A.L.; Mayhall, N.; Park, K. Multireference Ab Initio Studies of Magnetic Properties of Terbium-Based Single-Molecule Magnets. *J. Phys. Chem. A* **2019**, *123*, 6996–7006. [[CrossRef](#)]
127. Rinehart, J.D.; Fang, M.; Evans, W.J.; Long, J.R. A N<sub>2</sub><sup>3−</sup> Radical-Bridged Terbium Complex Exhibiting Magnetic Hysteresis at 14 K. *J. Am. Chem. Soc.* **2011**, *133*, 14236–14239. [[CrossRef](#)]
128. Rinehart, J.D.; Fang, M.; Evans, W.J.; Long, J.R. Strong Exchange and Magnetic Blocking in N<sub>2</sub><sup>3−</sup>-Radical-Bridged Lanthanide Complexes. *Nat. Chem.* **2011**, *3*, 538–542. [[CrossRef](#)]
129. Vieru, V.; Iwahara, N.; Ungur, L.; Chibotaru, L.F. Giant Exchange Interaction in Mixed Lanthanides. *Sci. Rep.* **2016**, *6*, 24046. [[CrossRef](#)]
130. Tretyakov, E.V.; Ovcharenko, V.I. The Chemistry of Nitroxide Radicals in the Molecular Design of Magnets. *Russ. Chem. Rev.* **2009**, *78*, 971. [[CrossRef](#)]
131. Vostrikova, K.E. High-Spin Molecules Based on Metal Complexes of Organic Free Radicals. *Coord. Chem. Rev.* **2008**, *252*, 1409–1419. [[CrossRef](#)]

132. Ovcharenko, V.I.; Vostrikova, K.E.; Romanenko, G.V.; Ikorski, V.N.; Podberezhskaya, N.V.; Larionov, S.V. Synthesis, Crystal Structure and Magnetic Properties of Di(Methanol) and Di(Ethanol)-Bis 2,2,5,5-Tetramethyl-1-Oxyl-3-Imidazoline-4-(3',3',3'-Trifluoromethyl-1-Propenyl-2'-Oxyato Nickel(II)—A New Type of Low Temperature Ferromagnetics. *Dokl. Akad. Nauk SSSR* **1989**, *306*, 115–118.
133. Meng, X.; Shi, W.; Cheng, P. Magnetism in One-Dimensional Metal–Nitronyl Nitroxide Radical System. *Coord. Chem. Rev.* **2019**, *378*, 134–150. [[CrossRef](#)]
134. Fegy, K.; Vostrikova, K.E.; Luneau, D.; Rey, P. New Nitroxide Based Molecular Magnetic Materials. *Mol. Cryst. Liq. Cryst. Sci. Technol. Sect. A. Mol. Cryst. Liq. Cryst.* **1997**, *305*, 69–80. [[CrossRef](#)]
135. Ovcharenko, V.I.; Vostrikova, K.E.; Ikorskii, V.N.; Larionov, S.V.; Sagdeev, R.Z. The Low Temperature Ferromagnet Dimethanol-Bis-[2,2,5,5-Tetramethyl-1-Oxyl-3-Imidazoline-4-(3',3',3'-TriFluoromethyl-1'-Propenyl-2'-Oxyato)] Cobalt(II),  $\text{CoL}_2(\text{CH}_3\text{OH})_2$ . *Dokl. Akad. Nauk SSSR* **1989**, *306*, 660–662.
136. Hintermaier, F.; Volodarsky, L.B.; Polborn, K.; Beck, W. New 2,5-Dihydroimidazole-1-Oxyls with Functional Side Groups (N, O, S Donors). *Liebigs Ann.* **1995**, *1995*, 2189–2194. [[CrossRef](#)]
137. Hintermaier, F.; Sünkel, K.; Volodarsky, L.B.; Beck, W. Synthesis, Structure, and Magnetic Properties of Transition Metal Complexes of the Nitroxide 2,5-Dihydro-4,5,5-Trimethyl-2,2-Bis(2-Pyridyl)Imidazole-1-Oxyl. *Inorg. Chem.* **1996**, *35*, 5500–5503. [[CrossRef](#)]
138. Perfetti, M.; Caneschi, A.; Sukhikh, T.S.; Vostrikova, K.E. Lanthanide Complexes with a Tripodal Nitroxyl Radical Showing Strong Magnetic Coupling. *Inorg. Chem.* **2020**, *59*, 16591–16598. [[CrossRef](#)]
139. Rey, P.; Smolentsev, A.I.; Vostrikova, K.E. Oxazolidine Nitroxide Transformation in a Coordination Sphere of the  $\text{Ln}^{3+}$  Ions. *Molecules* **2022**, *27*, 1626. [[CrossRef](#)]
140. Rey, P.; Caneschi, A.; Sukhikh, T.S.; Vostrikova, K.E. Tripodal Oxazolidine-N-Oxyl Diradical Complexes of  $\text{Dy}^{3+}$  and  $\text{Eu}^{3+}$ . *Inorganics* **2021**, *9*, 91. [[CrossRef](#)]
141. Köhn, R.D.; Pan, Z.; Kociok-Köhn, G.; Mahon, M.F. New Sandwich Complexes of Praseodymium(III) Containing Triazacyclohexane Ligands. *J. Chem. Soc. Dalton Trans.* **2002**, 2344–2347. [[CrossRef](#)]
142. Wedal, J.C.; Ziller, J.W.; Evans, W.J. Trimethyltriazacyclohexane Coordination Chemistry of Simple Rare-Earth Metal Salts. *Dalton Trans.* **2023**, *52*, 4787–4795. [[CrossRef](#)]
143. Hazama, R.; Umakoshi, K.; Kabuto, C.; Kabuto, K.; Sasaki, Y. A Europium(III)-N,N,N',N'-Tetrakis(2-Pyridylmethyl)-(R)-Propylenediamine Complex as a New Chiral Lanthanide NMR Shift Reagent for Aqueous Neutral Solution. *Chem. Commun.* **1996**, 15–16. [[CrossRef](#)]
144. Vostrikova, K.E.; Samsonenko, D.G. CCDC 2268033: Experimental Crystal Structure Determination. *CSD Commun.* **2023**. [[CrossRef](#)]
145. Ishida, T.; Murakami, R.; Kanetomo, T.; Nojiri, H. Magnetic Study on Radical-Gadolinium(III) Complexes. Relationship between the Exchange Coupling and Coordination Structure. *Polyhedron* **2013**, *66*, 183–187. [[CrossRef](#)]
146. Kanetomo, T.; Ishida, T. Strongest Exchange Coupling in Gadolinium(III) and Nitroxide Coordination Compounds. *Inorg. Chem.* **2014**, *53*, 10794–10796. [[CrossRef](#)]
147. Kanetomo, T.; Yoshitake, T.; Ishida, T. Strongest Ferromagnetic Coupling in Designed Gadolinium(III)–Nitroxide Coordination Compounds. *Inorg. Chem.* **2016**, *55*, 8140–8146. [[CrossRef](#)]
148. Hu, P.; Zhu, M.; Mei, X.; Tian, H.; Ma, Y.; Li, L.; Liao, D. Single-Molecule Magnets Based on Rare Earth Complexes with Chelating Benzimidazole-Substituted Nitronyl Nitroxide Radicals. *Dalton Trans.* **2012**, *41*, 14651. [[CrossRef](#)]
149. Wang, X.; Zhu, M.; Wang, J.; Li, L. Unusual Gd–Nitronyl Nitroxide Antiferromagnetic Coupling and Slow Magnetic Relaxation in the Corresponding Tb Analogue. *Dalton Trans.* **2015**, *44*, 13890–13896. [[CrossRef](#)]
150. Wang, J.; Miao, H.; Xiao, Z.-X.; Zhou, Y.; Deng, L.-D.; Zhang, Y.-Q.; Wang, X.-Y. Syntheses, Structures and Magnetic Properties of the Lanthanide Complexes of the Pyrimidyl-Substituted Nitronyl Nitroxide Radical. *Dalton Trans.* **2017**, *46*, 10452–10461. [[CrossRef](#)]
151. Benelli, C.; Caneschi, A.; Gatteschi, D.; Pardi, L. Gadolinium(III) Complexes with Pyridine-Substituted Nitronyl Nitroxide Radicals. *Inorg. Chem.* **1992**, *31*, 741–746. [[CrossRef](#)]
152. Hu, P.; Sun, Z.; Wang, X.; Li, L.; Liao, D.; Luneau, D. Magnetic Relaxation in Mononuclear Tb Complex Involving a Nitronyl Nitroxide Ligand. *New J. Chem.* **2014**, *38*, 4716–4721. [[CrossRef](#)]
153. Chen, P.Y.; Wu, M.Z.; Shi, X.J.; Tian, L. A Family of Multi-Spin Rare-Earth Complexes Based on a Triazole Nitronyl Nitroxide Radical: Synthesis, Structure and Magnetic Properties. *RSC Adv.* **2018**, *8*, 15480–15486. [[CrossRef](#)] [[PubMed](#)]
154. Nakamura, T.; Ishida, T. *Magnetic Exchange Interaction in Gadolinium(III) Complex Having Aliphatic Nitroxide Radical TEMPO*; AIP Publishing: New York, NY, USA, 2016; p. 020016.
155. Caneschi, A.; Dei, A.; Gatteschi, D.; Sorace, L.; Vostrikova, K. Antiferromagnetic Coupling in a Gadolinium(III) Semiquinonato Complex. *Angew. Chem. Int. Ed.* **2000**, *39*, 246–248. [[CrossRef](#)]
156. Zheludev, A.; Barone, V.; Bonnet, M.; Delley, B.; Grand, A.; Ressouche, E.; Rey, P.; Subra, R.; Schweizer, J. Spin Density in a Nitronyl Nitroxide Free Radical. Polarized Neutron Diffraction Investigation and Ab Initio Calculations. *J. Am. Chem. Soc.* **1994**, *116*, 2019–2027. [[CrossRef](#)]
157. Hamada, D.; Fujinami, T.; Yamauchi, S.; Matsumoto, N.; Mochida, N.; Ishida, T.; Sunatsuki, Y.; Tsuchimoto, M.; Coletti, C.; Re, N. Luminescent  $\text{Dy}^{\text{III}}$  Single Ion Magnets with Same N6O3 Donor Atoms but Different Donor Atom Arrangements, 'Fac'- $[\text{Dy}^{\text{III}}(\text{HL}^{\text{DL-Ala}})_3]\cdot 8\text{H}_2\text{O}$  and 'Mer'- $[\text{Dy}^{\text{III}}(\text{HL}^{\text{DL-Phe}})_3]\cdot 7\text{H}_2\text{O}$ . *Polyhedron* **2016**, *109*, 120–128. [[CrossRef](#)]

158. Murakami, R.; Nakamura, T.; Ishida, T. Doubly TEMPO-Coordinated Gadolinium(III), Lanthanum(III), and Yttrium(III) Complexes. Strong Superexchange Coupling across Rare Earth Ions. *Dalton Trans.* **2014**, *43*, 5893–5898. [[CrossRef](#)]
159. Tkachenko, I.A.; Petrochenkova, N.V.; Mirochnik, A.G.; Karasev, V.E.; Kavun, V.Y. Carboxylato-Bis-Dibenzoylmethanates of Europium(III): Luminescence and Magnetic Properties. *Russ. J. Phys. Chem. A* **2012**, *86*, 681–684. [[CrossRef](#)]
160. Kahn, M.L.; Sutter, J.-P.; Golhen, S.; Guionneau, P.; Ouahab, L.; Kahn, O.; Chasseau, D. Systematic Investigation of the Nature of the Coupling between a Ln(III) Ion (Ln = Ce(III) to Dy(III)) and Its Aminoxyl Radical Ligands. Structural and Magnetic Characteristics of a Series of {Ln(Radical)<sub>2</sub>} Compounds and the Related {Ln(Nitrone)<sub>2</sub>} Derivat. *J. Am. Chem. Soc.* **2000**, *122*, 3413–3421. [[CrossRef](#)]

**Disclaimer/Publisher's Note:** The statements, opinions and data contained in all publications are solely those of the individual author(s) and contributor(s) and not of MDPI and/or the editor(s). MDPI and/or the editor(s) disclaim responsibility for any injury to people or property resulting from any ideas, methods, instructions or products referred to in the content.